

Radiation Physics and Chemistry
Observation of Self-Healing and Blue Response Enhancement in c-Si Solar Cells
Exposed to Electron Irradiation
--Manuscript Draft--

Manuscript Number:	RPC-D-24-01859R2
Article Type:	Full Length Article
Section/Category:	Radiation Physics
Keywords:	Solar cell; Electron irradiation; Aged c-Si solar cell; Electrical characterization; Self-healing effect
Abstract:	The effects of electron irradiation on the performance of mono-crystalline silicon (c-Si) solar cells were investigated by examining various electron doses, ranging from 225 to 900 Gy, with an energy of 8 MeV. The study focused on dose-dependent degradation in cell behavior resulting from irradiation. Detailed analysis was conducted through dark and illuminated current-voltage (I-V) measurements, external quantum efficiency (EQE) measurements, capacitance-voltage (C-V) measurements, and conductance-voltage (G/ ω -V) measurements. The observed degradations were thoroughly analyzed, quantified, and discussed by comparing the results obtained from complementary electrical and optical characterizations of the cells before and after irradiation. The experimental findings indicated that the degradation in cell parameters was attributed to irradiation-induced defect formations in the base layer. However, the devices were found to be resilient to defect formations in the emitter and near the depletion edge of the base. After 52 months of irradiation, significant self-healing effects and improvements in blue response were observed in the cells, likely due to additional positive charge formation in the nitride layer from oxynitride formation in the ambient atmosphere over time, accelerated by radiation damage. This was confirmed by both illuminated I-V and EQE measurements.

REBUTTAL LETTER

Manuscript ID: RPC-D-24-01859

Reviewer #1: I am not ready to evaluate the manuscript positively.

The author has omitted responses to my (Reviewer 1) comments in the submitted manuscript.

The manuscript has a section "Response to Reviewer 1". However, it does not address my comments.

I confirm that none of the other response files contain references to my comments either.

I am attaching my comments along with the corresponding responses for you to look over. They don't match!!!

Thank you very much for your time and valuable feedback.

We would like to respectfully clarify a misunderstanding regarding your previous comments. During the first round of revision, we received four attachments via the editorial system; however, two of these attachments were identical and contained the same set of comments from another reviewer. Unfortunately, the file containing your specific comments was not among the materials forwarded to us by the journal at that time.

As a result, we were unaware of your original feedback and were therefore unable to address your suggestions in the first revision. Please rest assured that we carefully reviewed and responded to all comments provided in the files we received during the initial revision.

We sincerely apologize for any confusion this may have caused and emphasize that the lack of response to your comments was not due to any oversight or negligence on our part, but rather due to a likely error in the distribution of reviewer comments.

We are now pleased to respond fully to your valuable input in this revised version and have carefully addressed each of your comments below. We greatly appreciate your understanding.

C1) The study investigates changes in the ideality factor, determined by approximating experimental IV characteristics using a single-diode model. However, the description does not clarify whether shunt resistance R_{sh} was considered during the approximation. The changes observed in the IV curves presented in Fig. 1 might be linked to variations in R_{sh} value. Additionally, it is well known that a double-diode model is often more appropriate for silicon solar cells. The shape of the IV curves presented in Fig. 1 suggests that this approach may be more suitable. Furthermore, in the double-diode model, the ideality factor of each diode is associated with recombination processes occurring in distinct regions of the solar cell (the space-charge region and the quasi-neutral region). Therefore, applying the double-diode model to analyze the obtained results would be highly beneficial.

A1) Fig. 1 of the first uploaded manuscript became Fig. 2 in the first revision and it is also Fig. 2 in this new revised version of the manuscript.

We sincerely thank the reviewer for this insightful and constructive comment. We fully agree with the suggestion that the double-diode model provides a more accurate and physically meaningful framework for analyzing the dark I-V characteristics of silicon solar cells, especially for the cells relatively irradiated with higher dose level (675 Gy and 900 Gy) particularly considering the distinct recombination mechanisms occurring in the quasi-neutral and space-charge regions.

In response to the reviewer's valuable recommendation, we have revised our analysis accordingly. The previous single-diode model approach has been removed, and a full double-diode model analysis has been implemented throughout the dark I-V results section. The ideality factors (n_1 and n_2), saturation currents (I_{01} and I_{02}), series resistance (R_s), and shunt resistance (R_{sh}) have been extracted based on the double-diode model fitting.

Moreover, detailed discussions have been added to the ***Results and Discussion*** section to explain the physical significance of the two ideality factors and their relation to diffusion and recombination processes in different regions of the device. Special attention has also been given to the behavior of the shunt resistance (R_{sh}) as a function of electron dose and storage time, as suggested.

C2) Unfortunately, the study does not include the results of measuring the dark and illuminated IV curves of unirradiated solar cells before and after a 52-month at room temperature. The observed enhancement in blue response might not be related to the reconstruction of radiation-induced defects. Similar effects could result from changes in the defect structure introduced during solar cell fabrication or laser-based sample cutting.

A2) We sincerely appreciate the reviewer's insightful comment regarding the importance of comparing the dark and illuminated I-V curves of unirradiated solar cells before and after the 52-month period at room temperature. As suggested, we have included these measurements to clarify whether the observed enhancement in blue response could arise from intrinsic changes unrelated to radiation-induced defects.

The dark I-V curves for the unirradiated solar cell (0 months vs. 52 months) exhibit nearly identical trends, with minimal deviation in leakage current across the voltage range (-2.0 to 0.5 V). This consistency indicates negligible aging-related degradation in junction properties or defect activation under dark conditions.

Under illumination, the current density versus voltage curves (0 vs. 52 months) show no significant shift in key parameters (e.g., open-circuit voltage, fill factor). The overlap of these curves suggests that the solar cell's optoelectronic performance remains stable over time without laser-cutting or fabrication-induced artifacts.

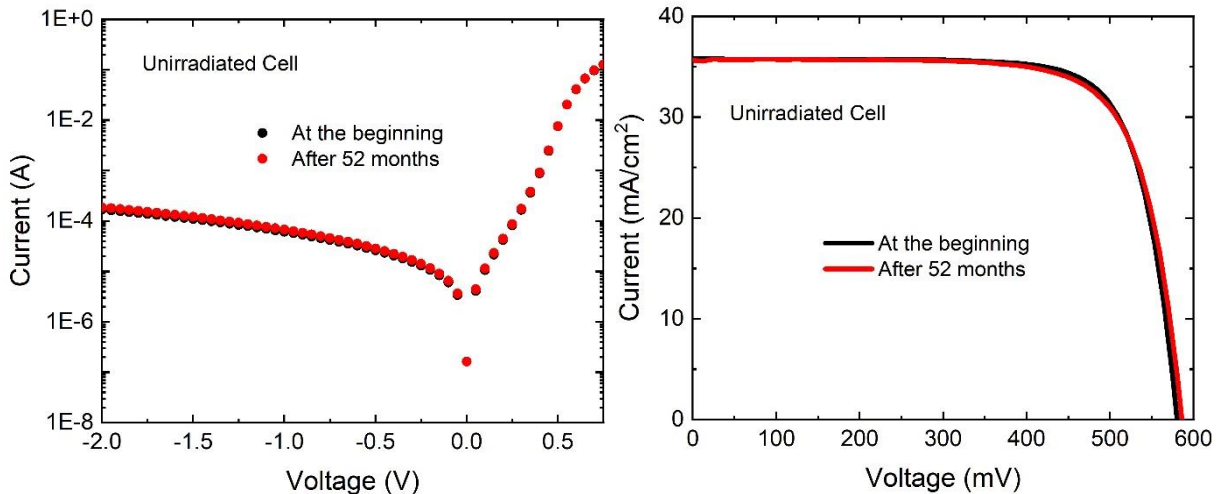


Figure: Dark and illuminated I-V curve of a un-irradiated cell at the beginning and after 52 months of storage at room temperature.

The I-V characteristics of the non-irradiated Si solar cells at 0 and 52 months, a clarifying sentence has been added to the manuscript:

“The dark and illuminated I-V characteristics of the non-irradiated Si solar cells at 0 and 52 months showed no noticeable differences (not shown here).”

C3) For electron irradiation at an energy of 8 MeV, uniform defect formation is expected throughout the 160 μm thick silicon layer. Why, then, are the changes in J_{sc} and V_{oc} attributed solely to the recombination centers in the base? Defects introduced in the emitter region would also be expected to influence the solar cell's performance.

A3) We appreciate the reviewer's insightful comment. It is indeed correct that 8 MeV electrons have sufficient energy to create a relatively uniform defect distribution throughout the entire silicon thickness, including both the emitter and base regions. Therefore, one would expect that defects introduced in the emitter could also impact solar cell performance, especially through increased surface or junction recombination.

However, based on our experimental observations, we conclude that the dominant contribution to the changes in J_{sc} and V_{oc} arises from recombination centers in the base region of the cells. As shown in Fig. 3, Figure 6 and Table 2, we observed a substantial degradation in both J_{sc} and V_{oc} just after electron irradiation across all dose levels. After 52 months of storage at room temperature, we observed partial recovery of these parameters whose recovery percentage depend on the dose levels. This long-term healing effect suggests that at least some of the radiation-induced defects are metastable and change it form either by dissociation or react with highly mobile vacancies and interstitials to change to more stable complexes or defect clusters. Such behavior is characteristic of bulk-related defect centers, such as divacancies and interstitial complexes, which are known to evolve over time even at room temperature. (Sufficient literature about expected defects due to irradiation and their reordering has been added to manuscript as response to comment 5). Without lacking supportive characterization techniques such as DLTS, TSC, EPR etc. We could only rely on literature suggestions and observation of cell parameters.

When looking to the EQE results (Figure 6 in the manuscript), it suggests that the base serves as the primary region for minority carrier transport and collection, it is inherently more sensitive to the introduction of recombination active centers as longer diffusion length requirement for the generated carriers far from the electric field region. Although the emitter may also contain radiation-induced defects, their impact is mitigated by the high P doping concentration ($\sim 5 \times 10^{20} \text{ cm}^{-3}$) and short carrier diffusion lengths in that region being very close to the electric field region. Moreover, the absence of persistent degradation in performance parameters after long-term storage further supports the view that defects in the emitter are either less impactful or more stable and thus did not dominate the observed trends. Even for the highest dose level there is no degradation in the collection efficiency of the carriers in the blue region when comparing EQE results of unirradiated and just after irradiation of cell responses. The degradation in charge collection starts about 535 nm of the spectrum with an absorption depth of around 1.1 – 1.3 μm from the surface, for the lowest dose level collection loss start about 650 nm with a corresponding absorption depth of about 3.5 μm . The junction depth of the cells is about 500 nm which is totally inside in this depth. The photons whose wavelength is less than about 450 nm are totally absorbed inside highly doped emitter region. Therefore, our observation suggests that carriers generated inside emitter layer collected without any loss just after irradiation even defect generation in the emitter layer. After 52 months of irradiation based on literature, we suggest the positive charge formation in nitrate layer to explain the blue response enhancement. We could not totally exclude the effects of defect transformation or reordering of the emitter for the enhancement of blue response, however we could not figure out possibility of this enhancement based on defect dynamics in the n+ emitter at room temperature for such long-time term without supportive characterization techniques (like DLTS, TCS, EPR etc). Our data indicates that the performance changes are primarily governed by recombination processes in the base. The potential influence of emitter defects is acknowledged, but based on our observations, it appears to play a secondary role in this context. Our findings are in line with previous studies on electron-irradiated silicon solar cells, where degradation and recovery trends were largely attributed to bulk defect dynamics rather than surface or emitter-layer effects (Ali et al., 2016; Babaee and Ghozati, 2017; Bhat et al., 2014; Curtin and Statler, 1975; Krishnan et al., 2007; Sathyanarayana Bhat et al., 2015; Srour and Palko, 2013; Yamaguchi et al., 1999; Zh Karazhanov, 2000).

C4) In the study, the enhancement in blue response is attributed to the formation of positive charges. However, it is unclear why the formation of these defects does not affect the barrier height, as the reverse C-V curves in Fig. 7 remain unchanged. Typically, the introduction of positive charges in the space-charge region would be expected to modify the barrier height, resulting in changes to the C-V characteristics. The authors should provide a clear explanation for why the observed enhancement in blue response is not accompanied by alterations in the barrier height, as indicated by the unchanged C-V curves.

A4) We sincerely thank the reviewer for this insightful and important comment. We would like to clarify the following:

- Fig. 7 of the first uploaded manuscript became Fig. 9 in the first revision and it is also Fig. 9 in this new revised version of the manuscript.

In our study, the enhancement in blue response after 52 months of storage is attributed to the increase of positive fixed charges in the silicon nitride (SiNx) passivation/antireflective layer, likely due to time-dependent ambient oxidation and possible oxynitride formation. These

additional positive charges could induce a field-effect passivation at the emitter surface, repelling minority carriers (holes) and reducing surface recombination losses. This surface passivation leads to improved carrier collection near the surface, particularly enhancing the short-wavelength (blue) response.

However, the C–V measurements primarily probe the space-charge region (SCR) properties of the p-n junction, determined by the doping profiles of the emitter and base regions. The positive charges in the SiNx reside outside the SCR and mainly modulate the surface potential without significantly altering the electric field or built-in potential across the main junction. Thus, the depletion capacitance, especially under reverse bias, remains largely unaffected, explaining the unchanged C–V curves due to charge formation in nitride layer. The high doping concentration of the n+ emitter reduces the sensitivity of the built-in potential to small surface potential changes. Since the depletion region extends mainly into the lower-doped p-base, the bulk capacitance remains the dominant factor, overwhelming any minor modulation induced by positive charges at the surface. Therefore, the enhancement in blue response is mainly attributed reduced surface recombination, while the C–V characteristics, which reflect the deeper bulk properties of the device, remain unaffected.

Additionally, due to the small size of the laser-cut cells (2.8 cm^2 from full wafer), the edge effects could be pronounced. The damaged edges and possible metallic residues can introduce extra recombination centers and local Fermi-level pinning, which may screen the effect of surface charges and dominate the electrical response, further suppressing any detectable modulation of the barrier height in C–V measurements.

C5) The defects that form in silicon during electron irradiation are well-documented. In my opinion, it is important to discuss which specific defects or defect reconstructions are responsible for the observed changes in photovoltaic parameters, such as radiation-induced degradation and the self-healing effect. A detailed analysis of the potential defects involved—such as the A-center, E-center, divacancies, and other radiation-induced defects—would provide a deeper understanding of the underlying mechanisms and significantly strengthen the study's conclusions.

A5) We thank the reviewer for this insightful and constructive comment. We agree that identifying and discussing the nature of specific irradiation-induced defects and their influence on photovoltaic parameters is important to fully understand the degradation and potential recovery mechanisms observed in silicon-based devices.

In response to this, we have expanded the ***Results and Discussion*** section by incorporating a more detailed explanation of the relevant defects and their roles in radiation damage and recovery. The origin of these defects lies in the displacement of atoms from their lattice positions during high-energy electron irradiation, resulting in the formation of vacancies, interstitials, and various complex defect structures (Radu et al., 2013; Srour et al., 2003). These defects are known to negatively affect carrier lifetimes and diffusion lengths, particularly in the base region of solar cells (Ashry and Fares, 2003; Bhat et al., 2014; Kuendig et al., 2003; Taylor et al., 1997).

Given the high energy of electrons (8 MeV) used in our study, we primarily expect complex defect structures involving vacancy–interstitial interactions and substitutional sites,

rather than isolated point defects. Well-documented complexes such as phosphorus–vacancy (P–V) and boron–oxygen interstitial (Bi–Oi) are particularly relevant. These defects are known to deactivate substitutional phosphorus and boron atoms, leading to dopant removal effects and a consequent increase in electrical resistance (Liao et al., 2023; Wunstorf et al., 1996; Zh Karazhanov, 2000). Additionally, both P–V and Bi–Oi complexes introduce deep-level traps; in particular, Bi–Oi pairs act as strong recombination centers due to their high electron capture cross-section (Schmidt et al., 1998; Svensson et al., 1997).

Furthermore, in Czochralski-grown silicon (Cz-Si), defects such as the oxygen–vacancy complex (A center), divacancy (V–V), carbon interstitial (Ci), and carbon–vacancy (C–V) complexes are known to form deep trap levels that significantly degrade cell performance after irradiation (Matsuura et al., 2006; Yamaguchi et al., 1999; Zh Karazhanov, 2000).

We also elaborated on the dynamic nature of these defects. Due to the high mobility of vacancies and interstitials at room temperature, irradiation-induced defects can undergo reconfiguration over time through dissociation or second-order reactions. For instance, Bi–Oi complexes may dissociate to form less effective recombination centers such as Bi–Cs, Bi–Bs, Bi–Oi–V, or eventually transform into Bs via secondary processes (Feklisova et al., 2013; Liao et al., 2024; Wunstorf et al., 1996; Yamaguchi et al., 1999). Similarly, A centers, divacancies, and K centers (carbon–oxygen-related complexes) may be annealed out or transformed into less active complexes through further interaction with mobile defects (Chen et al., 2024; Feick, 1997; Moll, 1999).

Finally, we emphasize that these defect transformation and reordering mechanisms depend on several factors including irradiation dose, electron energy, doping levels, and impurity concentrations (especially carbon and oxygen). Nonetheless, long-term room temperature storage allows partial self-recovery of the cell performance. This is mainly attributed to the gradual reduction of recombination-active defects and an associated increase in the minority carrier diffusion length, particularly in the base region of the cell (Chen et al., 2024; Srour et al., 2003).

These clarifications and literature-based analyses have been incorporated into the revised manuscript to provide a more comprehensive explanation of the underlying physical mechanisms driving radiation-induced degradation and recovery in silicon solar cells.

C6) A suggested improvement is to combine the data from Table 2 and Table 3 into a single table. This approach would enable a more concise and reader-friendly presentation of the results, facilitating direct comparisons.

A6) We sincerely appreciate the reviewer's constructive suggestion to merge Table 2 (basic cell parameters) and Table 3 (calculated loss/recovery in J_{SC}) into a single table for conciseness. However, we respectfully propose retaining the current separation for the following reasons:

Table 2 reports the essential photovoltaic parameters (V_{OC} , J_{SC} , FF, η) obtained from illuminated I-V measurements under three distinct irradiation states (unirradiated, just after irradiation, and after 52 months of irradiation). These parameters provide a comprehensive overview of the device's electrical performance across different radiation conditions.

In contrast, Table 3 presents derived quantities based specifically on J_{sc} values from Table 2—namely, the loss and recovery in J_{sc} and the corresponding recovery percentages. These are calculated metrics intended to analyze and quantify radiation-induced degradation and long-term recovery behavior, rather than directly measured cell parameters.

Merging the two tables would risk overcomplicating the presentation and potentially obscure the logical distinction between raw measurement data and post-processed analytical values. Keeping the tables separate ensures clarity, maintains the integrity of data interpretation, and allows the reader to more easily follow the methodology and progression from experimental results to calculated outcomes.

References

- Ali, K., Khan, S.A., MatJafri, M.Z., 2016. Improved radiation resistant properties of electron irradiated c-Si solar cells. *Radiation Physics and Chemistry* 125, 220–226.
<https://doi.org/10.1016/j.radphyschem.2016.04.015>
- Ashry, M., Fares, S., 2003. Diffusion length analysis and measurement in the base region of photodiodes. *Journal of Physics and Chemistry of Solids* 64, 2429–2431.
[https://doi.org/10.1016/S0022-3697\(03\)00285-3](https://doi.org/10.1016/S0022-3697(03)00285-3)
- Babaee, S., Ghozati, S.B., 2017. The study of 1 MeV electron irradiation induced defects in N-type and P-type monocrystalline silicon. *Radiation Physics and Chemistry* 141, 98–102. <https://doi.org/10.1016/j.radphyschem.2017.06.012>
- Bhat, P.S., Rao, A., Krishnan, S., Sanjeev, G., Puthanveettil, S.E., 2014. A study on the variation of c-Si solar cell parameters under 8 MeV electron irradiation. *Solar Energy Materials and Solar Cells* 120, 191–196. <https://doi.org/10.1016/j.solmat.2013.08.043>
- Chen, X.C., Li, L., Wang, M.Y., Ren, H., Liu, X.Q., Zeng, G., Yang, G.X., 2024. Carrier-induced formation of electrically active boron-interstitial clusters in irradiated boron-doped silicon. *J Appl Phys* 135, 055101. <https://doi.org/10.1063/5.0172704>
- Curtin, D.J., Statler, R.L., 1975. Electron Damage Review of Radiation Damage to Silicon Solar Cells. *IEEE Trans Aerosp Electron Syst AES-11*, 499–513.
<https://doi.org/10.1109/TAES.1975.308112>
- Feick, H., 1997. Radiation tolerance of silicon particle detectors for high energy physics. Hamburg.
- Feklisova, O. V., Yarykin, N.A., Weber, J., 2013. Annealing kinetics of boron-containing centers in electron-irradiated silicon. *Semiconductors* 47, 228–231.
<https://doi.org/10.1134/S1063782613020085>
- Krishnan, S., Sanjeev, G., Pattabi, M., 2007. 8 MeV electron irradiation effects in silicon photo-detectors. *Nucl Instrum Methods Phys Res B* 264, 79–82.
<https://doi.org/10.1016/j.nimb.2007.08.004>
- Kuendig, J., Goetz, M., Shah, A., Gerlach, L., Fernandez, E., 2003. Thin film silicon solar cells for space applications: Study of proton irradiation and thermal annealing effects on

the characteristics of solar cells and individual layers. *Solar Energy Materials and Solar Cells* 79, 425–438. [https://doi.org/10.1016/S0927-0248\(02\)00486-5](https://doi.org/10.1016/S0927-0248(02)00486-5)

Liao, C., Fretwurst, E., Garutti, E., Schwandt, J., Makarenko, L., Pintilie, I., Filip, L.D., Himmerlich, A., Moll, M., Gurimskaya, Y., Li, Z., 2023. Investigation of the Boron removal effect induced by 5.5MeV electrons on highly doped EPI- and Cz-silicon. *Nucl Instrum Methods Phys Res A* 1056, 168559. <https://doi.org/10.1016/j.nima.2023.168559>

Liao, C., Fretwurst, E., Garutti, E., Schwandt, J., Pintilie, I., Nitescu, A., Himmerlich, A., Moll, M., Gurimskaya, Y., Li, Z., 2024. Investigation of high resistivity p-type FZ silicon diodes after 60Co γ -irradiation. *Nucl Instrum Methods Phys Res A* 1061, 169103. <https://doi.org/10.1016/j.nima.2024.169103>

Matsuura, H., Iwata, H., Kagamihara, S., Ishihara, R., Komeda, M., Imai, H., Kikuta, M., Inoue, Y., Hisamatsu, T., Kawakita, S., Ohshima, T., Itoh, H., 2006. Si substrate suitable for radiation-resistant space solar cells. *Jpn J Appl Phys* 45, 2648–2655. <https://doi.org/10.1143/JJAP.45.2648>

Moll, M., 1999. Radiation damage in silicon particle detectors. Hamburg.

Radu, R., Fretwurst, E., Klanner, R., Lindstroem, G., Pintilie, I., 2013. Radiation damage in n-type silicon diodes after electron irradiation with energies between 1.5 MeV and 15 MeV. *Nucl Instrum Methods Phys Res A* 730, 84–90. <https://doi.org/10.1016/j.nima.2013.04.080>

Sathyaranayana Bhat, P., Rao, A., Sanjeev, G., Usha, G., Priya, G.K., Sankaran, M., Puthanveettil, S.E., 2015. Capacitance and conductance studies on silicon solar cells subjected to 8MeV electron irradiations. *Radiation Physics and Chemistry* 111, 28–35. <https://doi.org/10.1016/j.radphyschem.2015.02.010>

Schmidt, J., Berge, C., Aberle, A.G., 1998. Injection level dependence of the defect-related carrier lifetime in light-degraded boron-doped Czochralski silicon. *Appl Phys Lett* 73, 2167–2169. <https://doi.org/10.1063/1.122411>

Srour, J.R., Marshall, C.J., Marshall, P.W., 2003. Review of displacement damage effects in silicon devices. *IEEE Trans Nucl Sci* 50, 653–670. <https://doi.org/10.1109/TNS.2003.813197>

Srour, J.R., Palko, J.W., 2013. Displacement damage effects in irradiated semiconductor devices. *IEEE Trans Nucl Sci* 60, 1740–1766. <https://doi.org/10.1109/TNS.2013.2261316>

Svensson, B.G., Jagadish, C., Hallé, A., Lalita, J., 1997. Generation of vacancy-type point defects in single collision cascades during swift-ion bombardment of silicon. *Phys Rev B* 55, 10498. <https://doi.org/10.1103/PhysRevB.55.10498>

Taylor, S.J., Yamaguchi, M., Matsuda, S., Hisamatsu, T., Kawasaki, O., 1997. Investigation of carrier removal in electron irradiated silicon diodes. *J Appl Phys* 82, 3239–3249. <https://doi.org/10.1063/1.365631>

Wunstorf, R., Bugg, W.M., Walter, J., Garber, F.W., Larson, D., 1996. Investigations of donor and acceptor removal and long term annealing in silicon with different boron/phosphorus

ratios. Nuclear Instruments and Methods in Physics Research A 377, 228–233.
[https://doi.org/10.1016/0168-9002\(96\)00217-3](https://doi.org/10.1016/0168-9002(96)00217-3)

Yamaguchi, M., Khan, A., Taylor, S.J., Ando, K., Yamaguchi, T., Matsuda, S., Aburaya, T., 1999. Deep level analysis of radiation-induced defects in Si crystals and solar cells. J Appl Phys 86, 217–223. <https://doi.org/10.1063/1.370698>

Zh Karazhanov, S., 2000. Effect of radiation-induced defects on silicon solar cells. J Appl Phys 88, 3941–3947. <https://doi.org/10.1063/1.1290453>

- We report effects of electron irradiation on c-Si solar cells with varying electron doses.
- Irradiation effects studied through electrical and spectral response measurements in a complementary way.
- The performance of aged c-Si solar cells was investigated again after 52 months later.
- Room temperature self-healing effect was observed after 52-month period of irradiation.
- Remarkable enhancement was observed in the blue response of the cells after 52-month period compared to the unirradiated and just irradiated cell responses.

Observation of Self-Healing and Blue Response Enhancement in c-Si Solar Cells Exposed to Electron Irradiation

Ismail Kabacelik^{1*} Mustafa Kulakci^{2,3}

¹ Department of Medical Services and Techniques, Vocational School of Health Services, Bartın University, 74100, Bartın, Turkey

² Department of Physics, Eskisehir Technical University, 26470 Eskişehir, Turkey

³ Institute of Earth and Space Sciences, Eskisehir Technical University, 26470, Eskişehir, Turkey

Abstract

The effects of electron irradiation on the performance of mono-crystalline silicon (c-Si) solar cells were investigated by examining various electron doses, ranging from 225 to 900 Gy, with an energy of 8 MeV. The study focused on dose-dependent degradation in cell behavior resulting from irradiation. Detailed analysis was conducted through dark and illuminated current-voltage (I-V) measurements, external quantum efficiency (EQE) measurements, capacitance-voltage (C-V) measurements, and conductance-voltage (G/ω -V) measurements. The observed degradations were thoroughly analyzed, quantified, and discussed by comparing the results obtained from complementary electrical and optical characterizations of the cells before and after irradiation. The experimental findings indicated that the degradation in cell parameters was attributed to irradiation-induced defect formations in the base layer. However, the devices were found to be resilient to defect formations in the emitter and near the depletion edge of the base. After 52 months of irradiation, significant self-healing effects and improvements in blue response were observed in the cells, likely due to additional positive charge formation in the nitride layer from oxynitride formation in the ambient atmosphere over time, accelerated by radiation damage. This was confirmed by both illuminated I-V and EQE measurements.

Keywords: Solar cell; Electron irradiation; Aged c-Si solar cell; Electrical characterization; Self-healing effect

* Corresponding author: Ismail Kabacelik
E-mail address: ikabacelik@gmail.com

1. Introduction

Photovoltaic (PV) has been a fast-growing market for the last decades to close the gap in increasing electrical energy demand in a sustainable way by using solar energy as being the largest among renewable energy sources. Today, the PV industry is overwhelmingly dominated by c-Si technology with a market share of over 90% in terrestrial applications (Yu et al., 2022). Although c-Si cell technology was the pioneer of the space utilization of PV and has kept its dominance in this area for a long time, its dominance has been superseded by group III-V semiconductor cell technology. Recently, Si has regained significant interest due to the widespread progress in space and aerospace technologies, which require large-scale and relatively cost-effective installations. Highly efficient new cell technologies based on hybrid integration of Si and III-V technologies either by mechanical or wafer bonding techniques have been pursued to provide a viable solution for flourishing market requirements in a reliable and cost-effective way (Cariou et al., 2018; Medjoubi et al., 2021; Mizuno et al., 2022). Besides its cost-effectiveness, Si is a good alternative to Ge as a bottom cell due to its superior properties much suitable for space environment, such as mechanical robustness, radiation and temperature tolerances (Essig et al., 2017; Medjoubi et al., 2021; Sharma et al., 2022; Yu et al., 2022).

Solar cells used in space applications are exposed to high-temperature cycles, wide range of charged and uncharged radiations that adversely affect cell performances (Hamache et al., 2016; Kabacelik et al., 2017; Luft, 1964; Nikolić et al., 2015; Pellegrino et al., 2019; Sato et al., 2009; Yang et al., 2011). Therefore, cells to be used in that harsh environment inevitably require not only high-efficiency values with a high watt/kg ratio but also high tolerances to that hard condition for stable and long-term reliable use in space platforms. Today only a few material systems can provide all these requirements and prove themselves over long-term use in numerous different tasks. While c-Si cells show moderate sensitivity to radiation-induced degradation compared to thin-film and multi-junction cells, their widespread adoption, mature technology, and relatively low cost make them a practical choice in various radiation environments. When comparing c-Si solar cells with other types such as III-V group solar cells, Cu_x(In_{1-x}Ga)_{1-y}Se₂, CdTe/CdS, and perovskite solar cells for space applications, several key factors come into play, particularly in terms of efficiency, radiation hardness, cost-effectiveness, functionality over flexibility and lightweightness (Jasenek and Rau, 2001; Kawakita et al., 2002; Krishnan et al., 2009; Lang et al., 2016; Yang et al., 2020). c-Si solar cells, although widely used in terrestrial environments due to their cost-effectiveness and established manufacturing processes, exhibit moderate radiation resistance (Hamache et al., 2016; Mizuno et al., 2022). Their performance can degrade over time when exposed to high-energy space

radiation, leading to an increase in defect density and a reduction in carrier lifetime. In contrast, III-V group solar cells, known for their high efficiency, particularly in multi-junction configurations, are far superior in terms of radiation resistance (Li et al., 2021; Raya-Armenta et al., 2021). These cells are specifically designed to withstand the harsh radiation environment of space, maintaining their performance over extended periods. Cu(In,Ga)Se₂ solar cells, while flexible and efficient, offer higher radiation resistance than III-V cells (Jasenek and Rau, 2001; Kawakita et al., 2002). Consequently, their performance may deteriorate faster when subjected to the intense radiation in space. Similarly, CdTe/CdS solar cells, with a relatively simple manufacturing process and good efficiency, also show limited radiation tolerance (Verduci et al., 2022). This makes them less ideal for long-term missions in various radiation environments, where maintaining performance is critical. Perovskite solar cells, which have gained attention due to their high efficiency and lightweight properties, face challenges in terms of radiation resistance (Lang et al., 2016; Li et al., 2022; Yang et al., 2020). Their performance tends to degrade under prolonged exposure to space radiation, and their long-term stability is still under investigation.

As the irradiation by high energy particles introduces defect formations in solar cells (Srour et al., 2003; Zhang et al., 2020), it is critical to understand the behavior of the cells that are exposed to those radiations for the reliability and longevity of the utilization. Mainly two effects occur in the cell structure as a result of interaction with the energetic particles; the first one is ionization and the second one is displacement damage (Danilchenko et al., 2008; Summers et al., 1995; Zhang et al., 2014). The ionization effect is the generation of electron-hole pairs in the base layer of the cell. The displacement damage is the movement of atoms from their initial position in the crystal lattice to another position where they are electrically inactive. These induced defects produce generally deep energy levels in the band gap of the cell material (Ali et al., 2016; Nikolić et al., 2013). Then those defects mostly act as traps and recombination centers that cause to degradation in lifetime and diffusion length of minority carriers in the base of the cell and could cause to increased resistivity due to a reduction in the majority carriers (Bhat et al., 2014; Oeba et al., 2021; Yan et al., 2020; Zdravković et al., 2011). As a result of all effects, significant degradations could be observed in the output parameters of the cells (Hisamatsu et al., 1998; Shen et al., 2019; Tobnaghi et al., 2014; Weiss et al., 2020).

After successful demonstration on Vanguard I, Si cell had become the indispensable choice of cell technology for space applications for a long time (Essig et al., 2016; Green, 2016; Schnabel et al., 2020). To understand the effects of space conditions on Si cell performance, irradiation studies have been initiated as early as the 60s and keeping its importance up to date

(Junga and Enslow, 1959; Luft, 1964). Those studies that mimicking the space environment have led to the development of more tolerant Si cells in terms of design and material (Schygulla et al., 2022; Verduci et al., 2022). Although degradation mechanisms in Si cells are well understood with respect to different aspects of energetic particles like particle type, fluence, energy etc., there is a huge room about recovery after irradiation, especially on self-healing effects without applications of any external agents on the cells.

High-energy electron-induced degradation of Si solar cells has been extensively studied and reported in the literature (Ali et al., 2016; Babaee and Ghozati, 2017; Hamache et al., 2016; Kabaçelik, 2023; Liao et al., 2023; Sahin and Kabacelik, 2018; Yamaguchi et al., 1999). Yamaguchi et al. have observed a gradual decrease in I_{sc} under 1 MeV electron irradiation at fluences up to $5 \times 10^{16} \text{ e/cm}^2$, followed by a sharp decline to zero at a fluence of $1 \times 10^{17} \text{ e/cm}^2$ (Yamaguchi et al., 1996). Krishnan et al. reported a notable alteration in the diffusion component of the saturation current in Si photodetectors exposed to 8 MeV electron radiation at doses up to 100 kGy (Krishnan et al., 2007). It has been reported that fluences of 1 MeV electrons greater than 10^{16} cm^{-2} induce an anomalous increase in I_{sc} of Si solar cells, followed by a sudden decrease and cell failure, due to a decrease in carrier concentration in the base region and a reduction in the minority carrier diffusion length (Imaizumi et al., 1999). Bhat et al. have related the increase in the interface density of states in Si solar cells exposed to 8 MeV electron radiation to a decrease in carrier concentration, attributing this to the trapping of charge carriers caused by an increase in radiation-induced trap centers, as determined through C-V and G/w-V analyses (Sathyaranayana Bhat et al., 2015).

High-energy particle irradiation induces defects such as vacancies, interstitials, and complex structures mainly related with displacement of Si, oxygen (O), carbon (C), phosphorus (P), and boron (B) impurities (Feklisova et al., 2013; Liao et al., 2023; Matsuura et al., 2006). Prominent defect complexes include vacancy–carbon–oxygen ($\text{V}-\text{C}-\text{O}$), interstitial–carbon–interstitial–oxygen (C_i-O_i), interstitial–boron–interstitial–oxygen (B_i-O_i), and vacancy–oxygen–boron ($\text{V}-\text{O}-\text{B}$) complexes (Liao et al., 2023; Matsuura et al., 2006; Yamaguchi et al., 1999). Vacancy-related centers like the E-center ($\text{P}-\text{V}$), A-center ($\text{V}-\text{O}_i$), (B_i-O_i) and divacancy states ($\text{V}-\text{V}$) are assumed to be significant contributors to recombination losses (Radu et al., 2013; Yamaguchi, 2001; Zh Karazhanov, 2000). These defects adversely affect carrier lifetimes and increase recombination rates, underscoring the importance of understanding their formation and behavior to enhance solar cell resilience in high-energy environments, such as space.

In this study, the effects of 8 MeV electron irradiation on the c-Si solar cell performance have been investigated extensively and in detail for different doses. Electrical and optoelectronic characterization techniques have been used to evaluate the electron-induced degradations in the device characteristics of the cells before and after irradiation. After 52 months of irradiation cell parameters were measured again at the same conditions as before to reveal any possible effect of time. A remarkable self-healing effect has been observed in the cells kept at room temperature whose strength depends on electron dose and quantified through recovery in the cell parameters. The quantification of recovery in the cell parameters has been reached via comparative assessment of the successive measurement results of unirradiated and irradiated cells. Moreover, significant enhancement was observed in the blue response of the cells after 52 months of irradiation compared to that of unirradiated ones, which could shed a light to understand and develop new insights for the passivation of Si solar cells.

2. Materials and methods

The solar cells were fabricated using Czochralski-grown (Cz) mono-crystalline, (100) oriented, p-type Si wafer (boron-doped $\sim 5 \times 10^{16} \text{ cm}^{-3}$) with a resistivity of 1-3 $\Omega \cdot \text{cm}$, with a thickness of 160 μm , and with dimensions of 156 mm x 156 mm. The emitter layer (n) was formed by phosphorus diffusion with a concentration of $5 \times 10^{20} \text{ cm}^{-3}$. Details of the cell fabrication process are given elsewhere Ref (Es et al., 2016) and (Kulakci et al., 2013). A schematic diagram illustrating the overall structure of the fabricated solar cell used in this study is shown in Fig. 1.

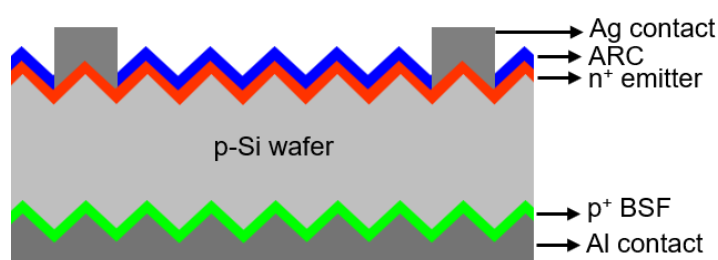


Figure 1. Schematic structure diagram of the fabricated Si solar cells.

Following the device fabrication, the cell was cut into smaller pieces with an area of 2.8 cm^2 by using a laser. Then, the electrical characteristics and spectral responses of each cell were measured before and after electron irradiation. The measurement done on irradiated cells after 1 day of irradiation and refers to just after irradiation in the text. Dark I-V measurements were performed by Keithley 2440 source-meter. Illuminated I-V measurements were performed

under AM1.5G condition using Abet 2000 solar simulator. The spectral response of the cells was measured in a wavelength range of 300 - 1100 nm and with an interval of 10 nm using Newport QuantX-300 quantum efficiency measurement system. C-V and G/ ω -V measurements were performed under dark conditions using an HP 4192A LF impedance analyzer, with an AC signal of 100 kHz frequency and 50 mV amplitude. All measurements were carried out at room temperature under atmospheric conditions (the pressure around 0.92 atm, humidity about 45%-50%).

Solar cells were exposed to electrons with an energy of 8 MeV using a modified clinical linear accelerator (cLINAC, Philips SLI-25 LINAC). In the cLINAC system, a 50 keV potential difference was applied to the electron gun to enable electron emission. The steering and focusing of the electrons, accelerated at approximately 3 GHz by radio frequency, are accomplished using standard magnetic and electrostatic components. The 8 MeV electron energy from the LINAC was directed at the solar cells with a uniform beam profile, which were positioned to face the beam directly to ensure that all samples received an equal irradiation dose. The dose rate was maintained constant at 7.5 Gy/min, provided the distance between the solar cell sample and the radiation source remained unchanged. Detailed information on cLINAC can be found at Ref (Boztosun et al., 2015). Four solar cells were chosen and separately irradiated with different doses of 225, 450, 675 and 900 Gy which are corresponding to 1.8×10^{14} to 7.2×10^{14} cm⁻² for the lowest and highest fluence of electron respectively. All irradiation processes were carried out under ambient conditions at room temperature.

In this study, electrical and optical properties of c-Si solar cells were systematically studied by means of dark and illuminated I-V, EQE, C-V and G/ ω -V measurements before and after 8 MeV electron irradiation at various applied doses. After irradiation solar cells were kept at ambient conditions at room temperature for 52 months and were characterized again to see possible recovery/degradation in time.

3. Results and discussions

Dark I-V characteristics of the solar cells were measured at room temperature before irradiation, just after irradiation, and after 52 months of room temperature storage for different electron doses (225 Gy, 450 Gy, 675 Gy, and 900 Gy). The experimental results are shown comparatively in Fig. 2. To analyze the I-V characteristics more accurately, the double diode model was employed. The double diode model expresses the total current as the sum of diffusion and recombination currents and is represented by the following equation (Krishnan et al., 2007; Wolf et al., 1977):

$$I = I_{01} \left[\exp \left(\frac{q(V - IR_s)}{n_1 kT} \right) - 1 \right] + I_{02} \left[\exp \left(\frac{q(V - IR_s)}{n_2 kT} \right) - 1 \right] + \frac{V - IR_s}{R_{sh}} \quad (1)$$

where I_{01} and I_{02} are the saturation currents corresponding to the diffusion in the bulk and generation-recombination in the space charge region, n_1 and n_2 are the diode ideality factors, R_s and R_{sh} are the series and shunt resistances, k is the Boltzmann constant and T is the temperature.

Before irradiation, the ideality factors n_1 and n_2 are close to 1.2–1.5 and 2, respectively. The slight elevation of the ideality factors could be attributed to minor surface recombination, pre-existing low level defect and laser damage of the cell edges. The deviation of the beginning cell parameters also could be due to laser cut process. Immediately after irradiation, there is an increase in both n_1 and n_2 which is more notable in n_2 indicating the formation of deep-level defects due to irradiation that enhance generation-recombination processes within the space-charge region (Bodunrin and Moloi, 2024; Oeba et al., 2024). After 52 months of room temperature storage, partial recovery is observed suggesting the self-annealing of certain radiation-induced defects over time. In overall the enhancement in n_2 is more remarkable compared to n_1 , which may suggesting that the defects formed in space charge region are more prone to self-annealing. Complex behavior observed in R_{sh} evolution, especially after high-dose irradiation where both irradiation-induced and laser-induced defect dynamics coexist. In addition to irradiation-induced effects, processing steps such as laser cutting can also influence the device behavior, particularly for small-area cells. The laser cutting process may introduce surface and subsurface damages, such as metal residues, silicon-metal phases, and microcracks, particularly near the cell edges. These damages increase the recombination probability and can create localized leakage paths, impacting both diffusion and recombination currents. Overall, these factors should be considered when interpreting the electrical characteristics of laser-cut, irradiated solar cells as here (Srour et al., 2003).

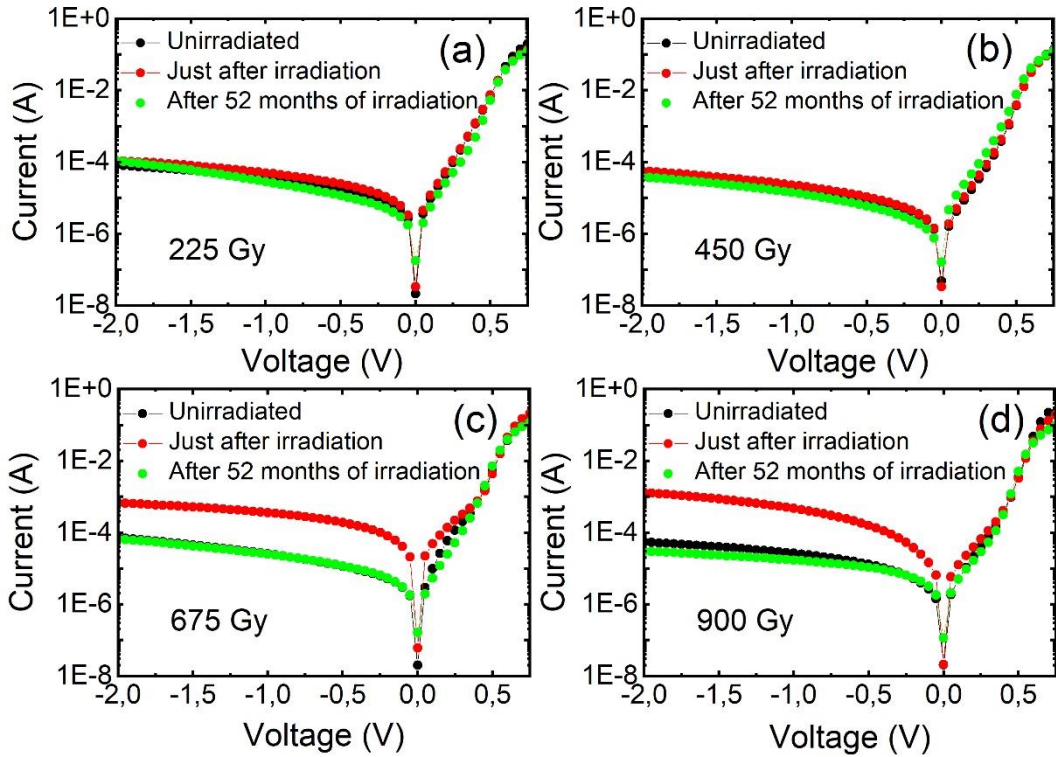


Figure 2. Dark I-V curves of silicon solar cells measured at room temperature for different doses of electron irradiation, showing evolution before irradiation, just after irradiation, and after 52 months of storage. The dark I-V characteristics of the non-irradiated Si solar cells at 0 and 52 months showed no noticeable differences (not shown here).

Table 1. Calculated diode parameters of the cells from measured dark I-V results.

Dose (Gy)	Unirradiated			Just after irradiation			After 52 months of irradiation		
	n ₁	n ₂	R _{sh} (Ω)	n ₁	n ₂	R _{sh} (Ω)	n ₁	n ₂	R _{sh} (Ω)
225	1.26	2.35	45561	1.34	2.51	13717	1.28	2.41	23797
450	1.28	2.37	58321	1.41	3.39	65316	1.41	2.36	85404
675	1.30	2.44	82353	2.00	3.92	4229	1.41	2.43	75404
900	1.47	1.65	3818	1.26	2.35	45561	1.43	2.31	22420

The illuminated I-V characteristics of solar cells under AM1.5G condition before and after irradiation with different electron doses are shown in Fig. 3. Calculated cell parameters using data of this figure are presented in Table 2. The mismatch in the results of different cells could be attributed to the effect of laser cut. The parameters of the full wafer cell before laser cut were 17.6 %, 612 mV, 36.1 mA/cm² and 79.7 % for η, Voc, J_{SC} and FF, respectively. The

laser cut induced edge degradation is clearly seen when comparing the cell parameters of full wafer cell and small cells used in this study. As clearly seen from figure and table, there is a reduction in both J_{SC} and V_{OC} values of cells after irradiation where the level of reductions follows an increase in electron dose. The decrease in J_{SC} and V_{OC} is due to the electron-induced defects that act as recombination centers for the light-generated carriers before diffusing to the depletion region. As the density of defects increases with the radiation dose, carrier loss becomes more pronounced in a monotonous way (Bodunrin and Moloi, 2022; Giesecke et al., 2011; Horiuchi et al., 2000), even for aggressively higher dose levels anomalous degradation in cell outputs could be observed (Morita et al., 1997). The origin of those defects is displacement of atoms from their lattice sites, creation of vacancies, interstitials and their complex structures due to interactions between them (Radu et al., 2013; Srour and Palko, 2013). These defects generally manifest themselves on the carrier's lifetime/diffusion length, especially in the base layer of the cells (Ashry and Fares, 2003; Bhat et al., 2014; Kuendig et al., 2003; Taylor et al., 1997).

Considering the energy of electrons (8 MeV) in this study, we expect complex structure of defects related to vacancy, interstitial and substitutional sites rather than isolated form of them being as point defects. Those of them, P–V and Bi_i – O_i are well known to cause dopant removal effect by de-activating substitutional B and P (Liao et al., 2023; Wunstorf et al., 1996; Zh Karazhanov, 2000). Dopant deactivation induced by these defects results in elevated electrical resistance within the cells. Besides dopant removal, P–V and Bi_i – O_i complexes introduce recombination levels; in particular, Bi_i – O_i pairs are considered highly effective recombination centers due to their large electron capture cross-section (Schmidt et al., 1998; Svensson et al., 1997). Moreover, in Cz-Si oxygen–vacancy pair (A center), divacancy (V–V), C_i and C–V complex are also well-known deep trap levels after high energy particle irradiation introducing recombination levels as effective as Bi_i – O_i (Matsuura et al., 2006; Yamaguchi et al., 1999; Zh Karazhanov, 2000). Over time, as vacancies and interstitials are quite mobile in Si, these defects undergo thermal reconfiguration even at room temperature due to dissociation and migration. First and second order reactions between them and between substitutional sites may cause to form new defect complexes, change in their concentration, change in their charge states and band gap activities (Chen et al., 2024; Feick, 1997; Schmidt et al., 1998; Srour et al., 2003).

After irradiation, cells were kept at ambient conditions at room temperature for 52 months to see any recovery/degradation in time. When looking at the comparative I-V curves in the figure, one can easily see varying self-recovery behavior in the cell parameters depending on radiation dose, which is more remarkable in the J_{SC} . The degree of improvement is the

greatest in the cell irradiated with the lowest dose of electron and is monotonously decreasing with the increase in dose level. Observed room temperature self-healing effects in the J_{SC} discussed in detail below together with EQE results. A small improvement was also observed in V_{OC} values, but it is not substantial as in the case of J_{SC} .

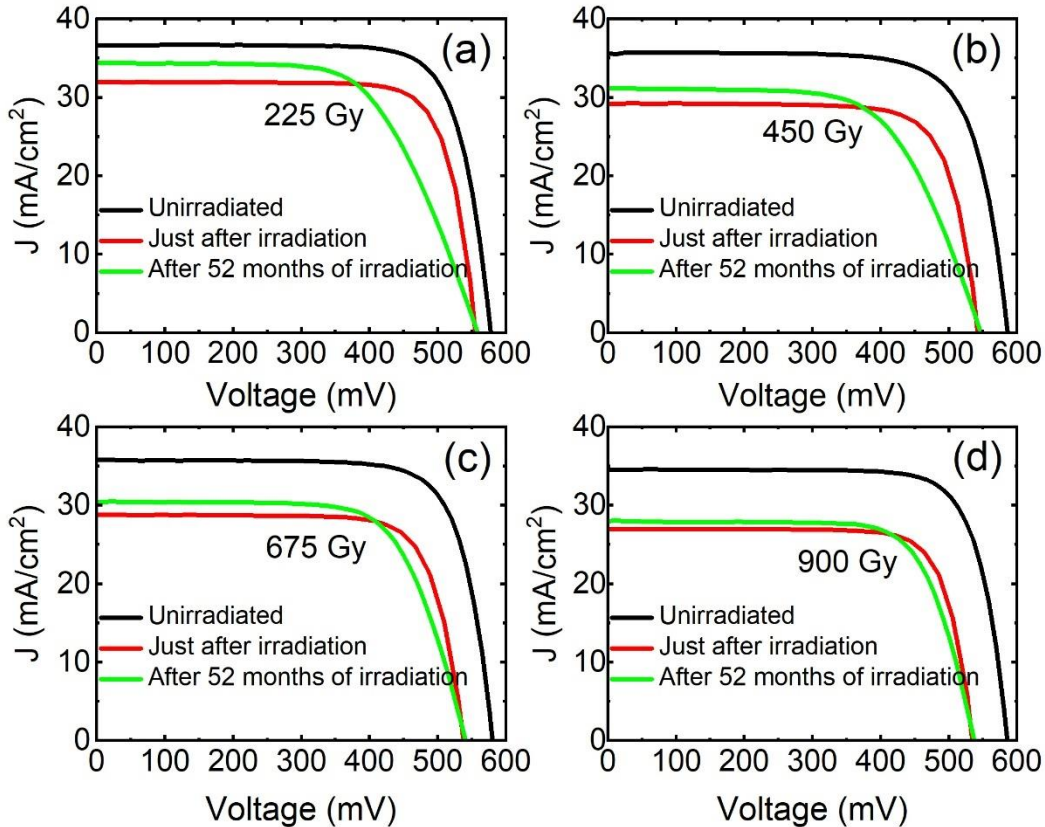


Figure 3. Illuminated (AM1.5G) I-V curves of the cells for different doses of electron irradiation. The illuminated I-V characteristics of the non-irradiated Si solar cells at 0 and 52 months showed no noticeable differences (not shown here).

Table 2. Basic cell parameters obtained from illuminated I-V given in Fig.3

Dose (Gy)	Unirradiated				Just after irradiation				After 52 months of irradiation			
	V_{OC} (mV)	J_{SC} (mA/ cm ²)	FF (%)	η (%)	V_{OC} (mV)	J_{SC} (mA/ cm ²)	FF (%)	η (%)	V_{OC} (mV)	J_{SC} (mA/ cm ²)	FF (%)	η (%)
225	578	36.7	77.1	16.3	553	31.9	78.7	13.9	558	34.4	62.9	12.1
450	586	35.6	74.9	15.6	542	29.3	76.5	12.1	546	31.2	63.7	10.8
675	580	35.8	76.5	15.9	538	28.8	76.7	11.9	540	30.4	69.5	11.4
900	585	34.6	77.8	15.7	534	26.9	78.4	11.3	537	27.9	73.4	10.9

The evolution of the tabulated cell parameters is visualized in Fig. 4 to easily follow the effects of electron dose on the performance of the cells. Fig. 4(a) shows the normalized parameters of just-irradiated cells; the normalization done on each irradiated cell parameters by their unirradiated values separately as each cell has nonequivalent device characteristics. The 0 Gy represents the normalization of unirradiated cell parameters by themselves separately for each cell as well. Therefore, Fig. 4 (a) represents the relative change of the cell parameters under varying irradiation dose with respect to their respective initial values. As seen in the figure, there is an obvious performance loss which increases with increasing dose level. The loss in conversion efficiency is 15% for the lowest dose level of 225 Gy and reaches 28% for the highest dose level of 900 Gy with respect to their initial values. The rate of efficiency loss goes to decrease with an increase in each successive dose level. It is observed that J_{SC} of the devices is more delicate to the electron irradiation compared to V_{OC} values. The loss in J_{SC} is 13% and 22% for the lowest and highest electron doses, whereas those loss are only 4% and 8% for V_{OC} for these subscribed dose levels respectively. Irrespective of the level of dose, the loss in efficiency is mainly determined by the degradation in J_{SC} rather than degradation in V_{OC} . Which could imply that irradiation is most effective in bulk region of the devices rather than surface or close surface regions. The degradation in cell parameters, especially in J_{SC} will be elaborated deeply with the conjunction of EQE measurement results. Any degradation has been observed in the FF values after irradiation, indeed slight enhancements are clearly seen. Similar behavior for FF-dose dependence was observed in Si solar cells irradiated with 8 MeV electron using much higher electron dose than that used here (Bhat et al., 2014).

1
2
3
4
5
6
7
8
9
10
11
12
13
14
15
16
17
18
19
20
21
22
23
24
25
26
27
28
29
30
31
32
33
34
35
36
37
38
39
40
41
42
43
44
45
46
47
48
49
50
51
52
53
54
55
56
57
58
59
60
61
62
63
64
65

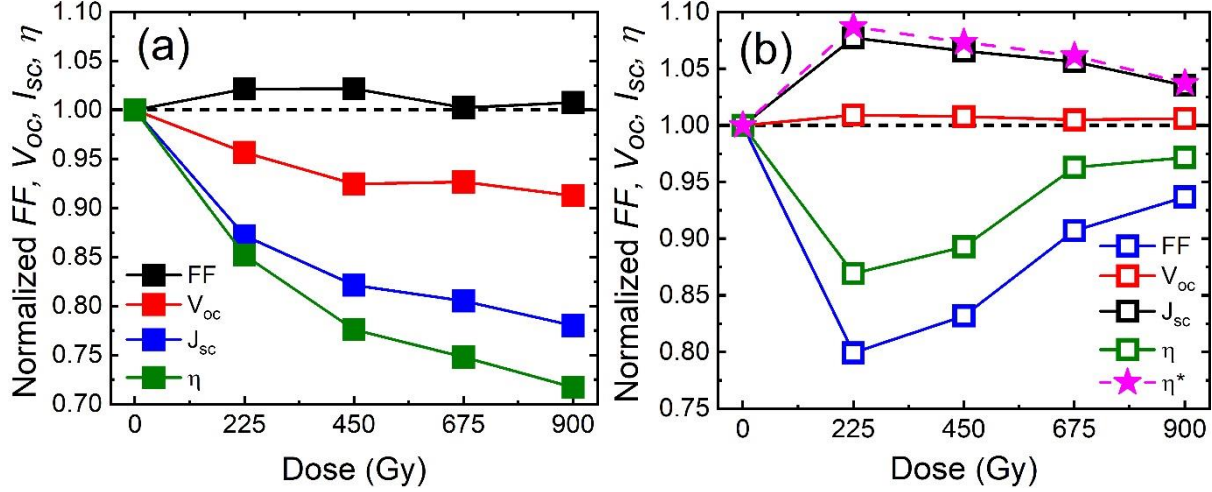


Figure 4. Evolution of normalized cell parameters: **(a)** values of just irradiated case, normalized by their unirradiated values, **(b)** values of after 52 months of irradiation, normalized by just irradiated values. The dashed lined curve in **(b)** represents the projected normalized efficiency (η^*) of the cells after 52 months, under the assumption FF values of just irradiated cells were preserved without any degradation.

Fig. 4(b) shows the normalized parameters of the cells measured after 52 months of irradiation. Normalizations were done on each parameter of the cells obtained after 52 months of irradiation with respect to their just irradiated values. In this case normalization is done to see the relative changes in the cell parameters after 52 months of irradiation compare to their just irradiated values. The 0 Gy represents the normalization of just irradiated cell parameters with themselves separately for each cell as well. When looking at the change in V_{oc} and J_{sc} values, the enhancement is seen compared to the just irradiated values. Which indicates room temperature self-healing effect in the cells without applying any external agent like heat treatment etc., the cells were only preserved in ambient conditions for 52 months. As clearly seen, there is a remarkable recovery in J_{sc} values which could imply that some of the defects generated in the bulk due to irradiation, especially those that are not very stable had been cured over the 52 months period (Bhat et al., 2014; Radu et al., 2013). The observed recovery is more pronounced in J_{sc} values compared to the recovery seen in the V_{oc} values. The relatively small amount of enhancement seen in the V_{oc} values is almost independent of the irradiation dose. On the other hand, the relative enhancement in J_{sc} is inversely proportional to the dose level. The maximum level of enhancement in current is seen in the cell that was irradiated with the lowest amount of electron dose, then the percentage of recovery decreases monotonously with an increase in electron dose. The calculated percentage recovered part of J_{sc} values due to self-healing is given in Table 3. The recovery in J_{sc} is 16.2% for the highest irradiation dose, it

monotonously increases with decrease in dose level and reaches as high as 52.6% for the lowest dose. More details on the recovery in current will be given in the EQE part. Although one expects enhancement in the conversion efficiencies (compared to just irradiated values) regarding the recovery in corresponding V_{oc} and J_{sc} values, the calculated efficiency values do not reflect the expectations as seen in Fig. 4(b). The reduction in efficiencies after 52 months solely depends on the degradation in FFs. As clearly seen in the figure, the efficiency-dose curve directly follows the behavior of FF-dose curve with almost the same functional dependence. The main reason for FF degradation after 52 months of irradiation was found to be an increase in the series resistance of the cells (Fig. 5). The shunt resistances had insignificant changes after 52 months compared to ones obtained from the measurements just done after irradiation of the cells (not shown here), this may be due to screening effect of the degraded cell edges by laser cut. For the case just after irradiation, series resistance slightly increases with an increase in dose level which could be expected due to increase in dopant removal probably caused by P-V for n-type region and B_i-O_i defects for p-type region. In a long-term annealing at room temperature partial recovery in dopant was observed for n- and p-type Si wafers irradiated with neutron (Wunstorf et al., 1996). Although we expected similar dopant annealing in our devices, the series resistance after 52 months increased compared to their just irradiated case. The increase in resistance after 52 months of irradiation could be due to degradation of contact materials and contact-Si interfaces. Contrary to just-irradiated cells behavior, the series resistance decreases in a monotonous way with an increase in irradiation dose (See Fig. 5). Assuming that, the FF of the irradiated cells were preserved without any degradation during this 52-month period, the projected conversion efficiencies were calculated and are shown as a dashed curve in Fig. 4(b). Based on this projection, efficiency losses caused by irradiation partially recovered, with 8.7% recovery for the lowest dose and 3.7% for the highest dose. Notably, the improvement in efficiency is primarily attributed to the recovery of the short-circuit current, as evidenced by the comparison between the current-dose and efficiency-dose curves in Fig. 4(b) across different irradiation levels.

1
2
3
4
5
6
7
8
9
10
11
12
13
14
15
16
17
18
19
20
21
22
23
24
25
26
27
28
29
30
31
32
33
34
35
36
37
38
39
40
41
42
43
44
45
46
47
48
49
50
51
52
53
54
55
56
57
58
59
60
61
62
63
64
65

1
2
3
4
5
6
7
8
9
10
11
12
13
14
15
16
17
18
19
20
21
22
23
24
25
26
27
28
29
30
31
32
33
34
35
36
37
38
39
40
41
42
43
44
45
46
47
48
49
50
51
52
53
54
55
56
57
58
59
60
61
62
63
64
65

Table 3. Calculated loss and recovery in J_{SC} values from illuminated I-V measurements (Fig. 3) for different radiation doses. J_{SC0} , J_{SC1} and J_{SC2} are the short circuit current densities of the cells before irradiation, just after irradiation and after a 52-month period of irradiation respectively.

Dose (Gy)	Loss in J_{SC} ($J_{SC0} - J_{SC1}$) (mA/cm ²)	Recovery in J_{SC} ($J_{SC2} - J_{SC1}$) (mA/cm ²)	Percentage in J_{SC} recovery (%)
225	4.70	2.47	52.6
450	6.37	1.92	30.1
675	6.97	1.62	23.2
900	7.60	1.23	16.2

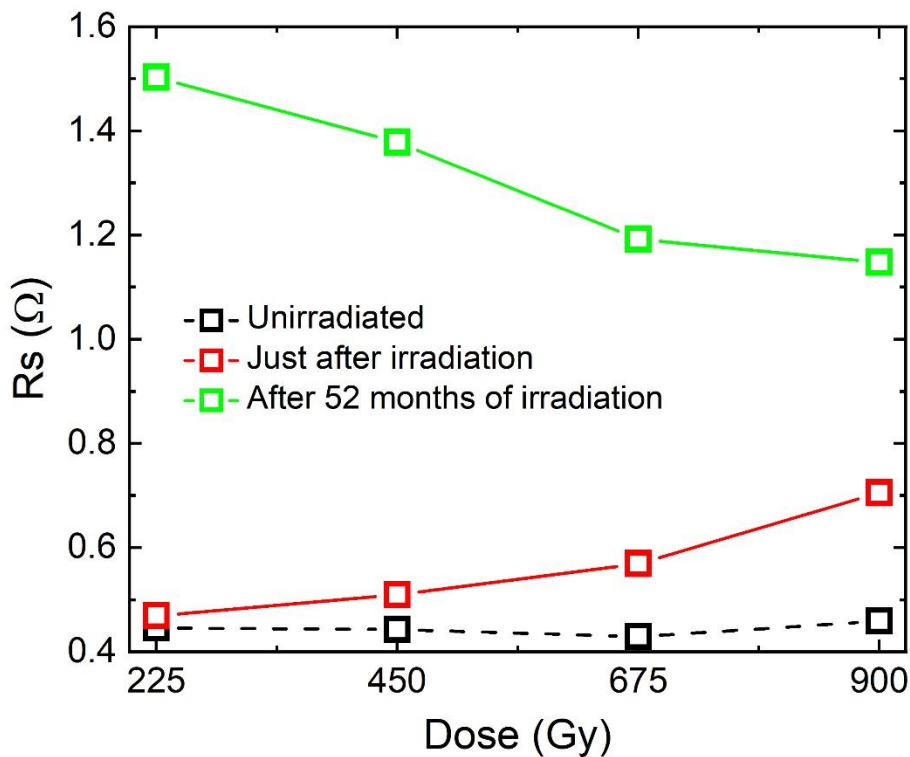


Figure 5. Irradiation effects on series resistance of the cells with varying electron doses from illuminated I-V measurements.

EQE measurement is a valuable method to understand the behavior of the cell with respect to specific region of incoming photon wavelength. To thoroughly investigate the degradation effects of electron irradiation on the cells and to determine the potential mechanisms responsible for the self-healing effects observed in the recovery of short circuit current, EQE measurements were conducted. The findings of these measurements are presented comparatively in Fig. 6.

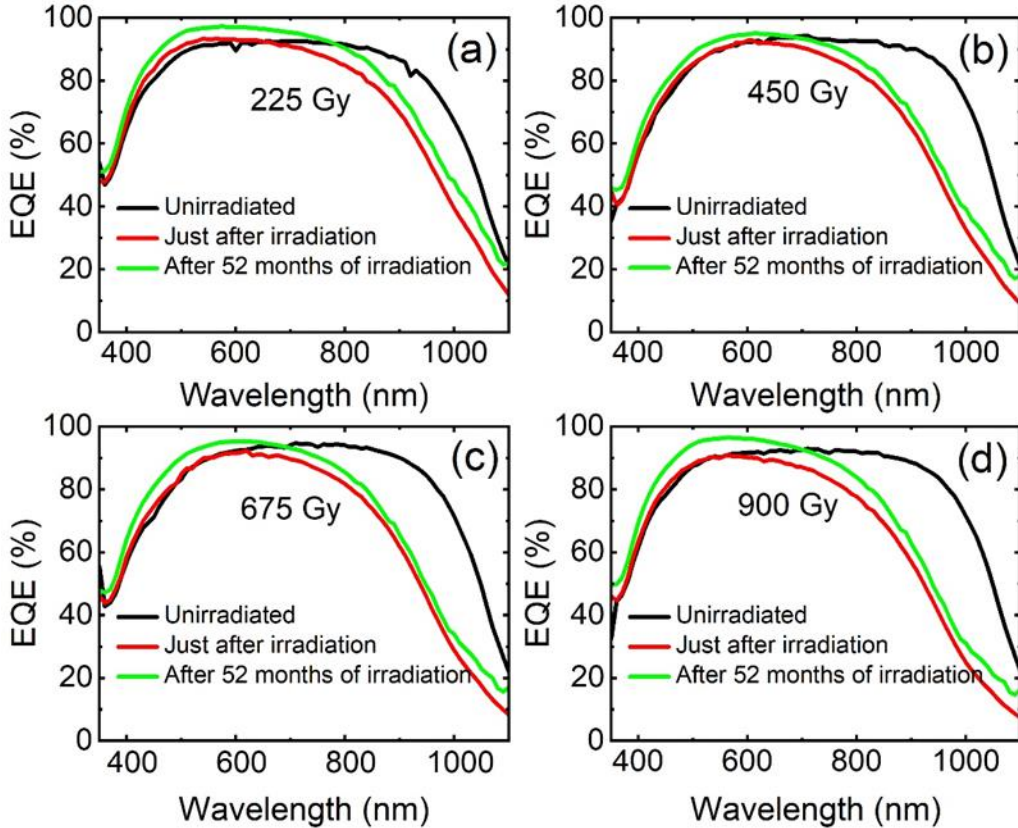


Figure 6. The EQE spectrum of the cells for different irradiation levels.

Based on the results shown in Fig. 6, a significant decrease in EQE values can be observed in the long-wavelength region of the spectrum, and this loss in the red response becomes more prominent with increasing levels of irradiation. It is noteworthy that electron irradiation did not cause any changes in the reflectivity properties of the cells. To see any effect of storage for 52 months on the cell behavior, EQE of unirradiated another cell is given in Fig. 7(inset). Any observable changes (degradations or enhancements) were detected in the EQE results of an unirradiated cell measured at the beginning of the study and after 52 months. Therefore, the reductions in EQE (Fig.6) are directly attributed to the decline in carrier collection due to defects generated by irradiation in the active regions of the devices. On the other hand, EQE results suggest that solar cells have high tolerance to defects in the blue response region of the spectrum as the light absorbed close to the surface.

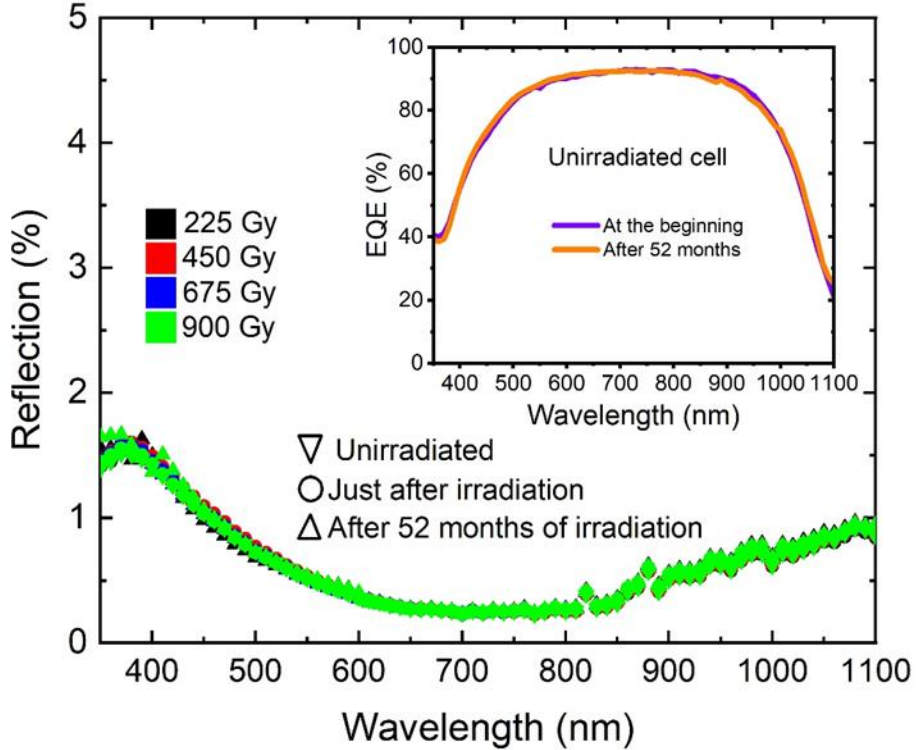


Figure 7. Comparative reflection spectrum of the cells. The inset shows the EQE spectrum of an unirradiated sample at the beginning and after 52 months.

Upon examination of Fig. 6, a distinct demarcation can be observed on the high-energy side of the curves. Beyond this point, towards the lower wavelength region of the spectrum, no detrimental effects on the cell response were observed. In fact, a very slight improvement can be seen in the curves. For the lowest dose (225 Gy), the border of onset is approximately at a wavelength of 654 nm, while for higher doses, this onset systematically shifts towards lower wavelengths and reaches around 535 nm for the highest irradiation dose (900 Gy). Considering the absorption depth of these wavelengths of light in Si, the onset points, at which the loss of minority carrier collection begins, are situated at approximately 3.5 μm from the surface of the cells for the lowest dose, and this depth decreases to around 1.1 μm for the highest dose. The cells have an emitter depth of 500 nm, and the depletion layer width in the absorber region is calculated to be around 300 nm. This indicates that for the highest irradiation dose, recombination loss begins in the immediate vicinity of the depletion region, and as the dose decreases, the loss moves deeper into the absorber. Based on the behavior of the curves, it can be inferred that there is no carrier loss observed in the emitter and depletion layers, even when subjected to the highest dose of electron irradiation, as compared to the response of unirradiated cells. The EQE results suggest that the degradation observed in the solar cells after electron irradiation can be attributed to the formation of defects in the base layer (Bhat et al., 2014;

Yamaguchi, 2001). These defects cause a reduction in the minority carrier diffusion length or minority carrier lifetime, resulting in carrier collection loss due to recombination (Babae and Ghozati, 2017). In the EQE results, the decrease in efficiency for longer wavelength photons in the spectrum is mainly attributed to absorption deeper in the absorber layer and towards the back contact, which results in significant loss of carrier collection, and this loss behavior is found to depend on the irradiation dose (Khan et al., 2003; Krishnan et al., 2007; Matsuura et al., 2006). The observed carrier loss behavior in EQE is well-correlated with the dose dependence of J_{sc} values obtained from the illuminated I-V curve of the cells just after irradiation (see Fig. 3, Fig. 4, and Table 3).

Fig. 6 also shows the EQE measurement results of the cells after 52 months of irradiation. There is an enhancement in the EQE response for all dose values across the entire spectrum compared to the results obtained immediately after irradiation. A significant increase in the blue response of the cells is observed in the curves, which is even higher than the blue response of the unirradiated cells. This enhancement in blue response could be due to the formation of positive charges in the silicon nitride layer over time, which might cause field effect passivation on the emitter surface by pushing minority carriers (holes) away from the interface. It is well known that excess positive charges related with K (+) center in silicon nitride serve as an effective field-effect passivation in silicon solar cells especially on n-type emitter (Leguijt et al., 1996; Lelièvre et al., 2009; Sharma et al., 2013). At room temperature, ambient oxidation could form oxynitride formation in silicon nitride film which enhances extra positive charge formation over oxygen-correlated bond defects in time which may boost field effect passivation over 52 months period (Raider et al., 1976; Schmidt and Aberle, 1999). Most probably due to radiation-induced damages this charge formation could be boosted and result in good surface passivation which is not observed in unirradiated cell (Robertson, 1993). Upon examining Fig. 6, it can be observed that the onset of carrier loss shifts to higher wavelengths compared to the results immediately after irradiation, with the switch occurring from around 654 nm to 786 nm for the lowest dose and from about 535 nm to 700 nm for the highest dose. In terms of the absorption depth of these wavelengths, the onset of carrier loss shifts from 3.5 μm to 9.6 μm for the lowest dose and from 1.1 μm to 5.0 μm for the highest dose, respectively. For doses in between, the recovery in EQE response is slightly lower compared to these extremes. The EQE curves suggest that the improvements in carrier collection could be attributed to the reordering of radiation-induced defects over time at room temperature, which could be referred to as the room temperature annealing or self-healing effect. It is well known that the vacancies and interstitials could easily move in Si structure at room temperature. Over

the time irradiation induced defects could be transformed into new complexes by reactions of vacancies and interstitials or dissociation of less stable more active defects to more stable less active defects. For example, recombination center Bi–O_i defect which is also responsible to acceptor removal could be dissociated to form less effective recombination center Bi–C_s, Bi–B_s, Bi–O_i–V defects or by second order reactions to B_s (Feklisova et al., 2013; Liao et al., 2024; Wunstorf et al., 1996; Yamaguchi et al., 1999). Also, other recombination centers such as A center (V-O_i), divacancy center (V-V) and K centers (carbon oxygen related complexes) could be annealed out by dissociation or by forming more complex structures through interactions with other vacancies and interstitials (Chen et al., 2024; Feick, 1997; Moll, 1999; Zh Karazhanov, 2000). Defect reordering or transformation processes would also depend on irradiation dose level, irradiation energy, doping level of wafer, and impurity concentrations (C, O) via concentration of produced vacancy and interstitial atoms. Nonetheless, on average some portion of generated defects recovered over long-term storage at room temperature and partial recovery in the cell performance has been observed mostly due to minority carrier diffusion length enhancement especially in the base layer. The enhancement and partial recovery in EQE over 52 months (Fig. 6) are consistent with the recovery in short-circuit current behavior (Fig. 3 and Fig. 4) obtained from illuminated I-V measurements.

As the EQE is the spectral distribution of photocurrent, short circuit current values of the cells also calculated using Eq. 2.

$$J_{sc} = \int EQE(\lambda) J_{\gamma,AM1.5G}(\lambda) d\lambda \quad (2)$$

where, $J_{\gamma, AM1.5G}(\lambda)$ is the incident photon current density per wavelength interval, derived from AM1.5G data taken from ASTM G173-03 reference spectrum.

To determine the loss and the self-healing effects in currents, the J_{sc} values calculated from EQE curves of cells for the cases of unirradiated, just irradiated, and after 52 months of irradiation are compared in Table 4, in a similar way as done in the illuminated I-V measurements. As seen from the table, the irradiation loss in current increases monotonously with an increase in dose level which is consistent with results that were obtained from the solar simulator measurements (Table 3). However, the degree of current losses measured under a solar simulator is slightly higher than ones calculated from EQE measurements. Based on the calculations using EQE spectrum, in a 52-month period after irradiation, 81.5% of the loss in current recovered back for the device subject to the lowest electron dose and it is about 44.3% for the highest dose respectively. For the dose levels in between them, the calculated recovery

in current is relatively low compared to these extremes. The recovery in short circuit currents calculated from EQE measurements is higher than that obtained from solar simulator measurements (Table 4 and Table 3). The differences observed loss in current levels just after irradiation and recovery in currents due to self-curing effects between the solar simulator and EQE measurement might be results of difference in illumination area on the cells. In solar simulator measurements the whole area of the cells was illuminated, on the other hand in EQE measurements the illumination area was only 2 mm². The cells used here are laser cut from a 243 cm² cell into a small size of 2.8 cm². The laser cut processing unavoidably damages the edges of the cells, which could introduce extra recombination and leak pathways, and this could lower the current in solar simulator measurement due to extra carrier losses over the defective edges.

Table 4. Calculated loss and recovery in J_{SC} values from EQE measurements (Fig. 6) for different radiation doses. J_{SC0}, J_{SC1} and J_{SC2} are the short circuit current densities of the cells for unirradiated, just irradiated and after 52 months of irradiation cases respectively.

Dose (Gy)	Loss in J _{SC} (J _{SC0} – J _{SC1}) (mA/cm ²)	Recovery in J _{SC} (J _{SC2} – J _{SC1}) (mA/cm ²)	Percentage in J _{SC} recovery (%)
225	2.75	2.24	81.5
450	4.62	1.73	37.4
675	5.36	1.89	35.3
900	5.87	2.60	44.3

As discussed earlier, there is a partial recovery in the carrier collection efficiency for the long-wavelength region compared to the significant enhancement observed in the short-wavelength region. For long wavelengths, where carriers are generated deeper within the bulk of the material, the collection efficiency is primarily governed by the minority carrier diffusion length (L). Using the EQE curve, the diffusion length for medium and long wavelengths can be calculated using Eq. 3 (Basu et al., 1994; Onoda et al., 2002; Saad, 2002).

$$\eta = (1 - R) \left(1 - \frac{e^{-\alpha W}}{1 + \alpha L_n} \right) \quad (3)$$

Here R is the reflection coefficient, α is the absorption coefficient, W is the depletion width and L_n is the minority carrier (electron) diffusion length.

The calculated minority carrier diffusion lengths for the cells are presented in Fig. 8 for wavelengths of 800 nm and 900 nm. The data clearly reveal variations in the diffusion length

1 among samples, which is attributed to the inhomogeneities introduced by the laser cutting
2 process used to divide the full wafer into individual cells. These inhomogeneities likely result
3 in differences in the bulk and surface recombination characteristics across the samples.
4

5 To account for such variations, the results of each sample were analyzed individually,
6 as was done for the I-V and EQE measurements. By evaluating each cell independently, we
7 eliminate the confounding effects of sample-to-sample inconsistencies and focus on the relative
8 changes in diffusion length under different conditions. Table 5 summarizes the relative
9 percentage changes in diffusion length for each sample, offering a more reliable basis for
10 comparison. It is observed that the diffusion length consistently increases as the wavelength
11 changes from 800 nm to 900 nm. This result aligns with theoretical expectations since longer
12 wavelengths penetrate deeper into the bulk of the Si, where the generation rate of carriers
13 decreases, making the measurement more sensitive to the bulk diffusion length (Honsberg and
14 Bowden, 2019).
15

16 Comparing the unirradiated state, the immediate post-irradiation state, and the 52-month
17 post-irradiation state, it is evident that irradiation induces a significant reduction in diffusion
18 length, consistent with the introduction of radiation-induced defects that act as recombination
19 centers. However, over time, a partial recovery in diffusion length is observed for both 800 nm
20 and 900 nm wavelengths. This room temperature recovery could be attributed to the annealing
21 of some radiation-induced defects or a reduction in their recombination activity under ambient
22 storage conditions.
23

24 The degree of recovery is more pronounced for the long-wavelength measurements (900
25 nm), suggesting that bulk recombination processes are more affected by defect annealing than
26 surface recombination. These results highlight the critical role of diffusion length as a parameter
27 for assessing the impact of irradiation and subsequent recovery in Si solar cells. The observed
28 trends in diffusion length across different wavelengths and irradiation conditions provide
29 valuable insights into the material's bulk properties and the long-term effects of radiation-
30 induced defects. These findings underscore the importance of independently analyzing each
31 sample and considering relative changes to draw reliable conclusions, particularly when dealing
32 with inhomogeneous samples such as those cut from a full wafer.
33
34
35
36
37
38
39
40
41
42
43
44
45
46
47
48
49
50
51
52
53
54
55
56
57
58
59
60
61
62
63
64
65

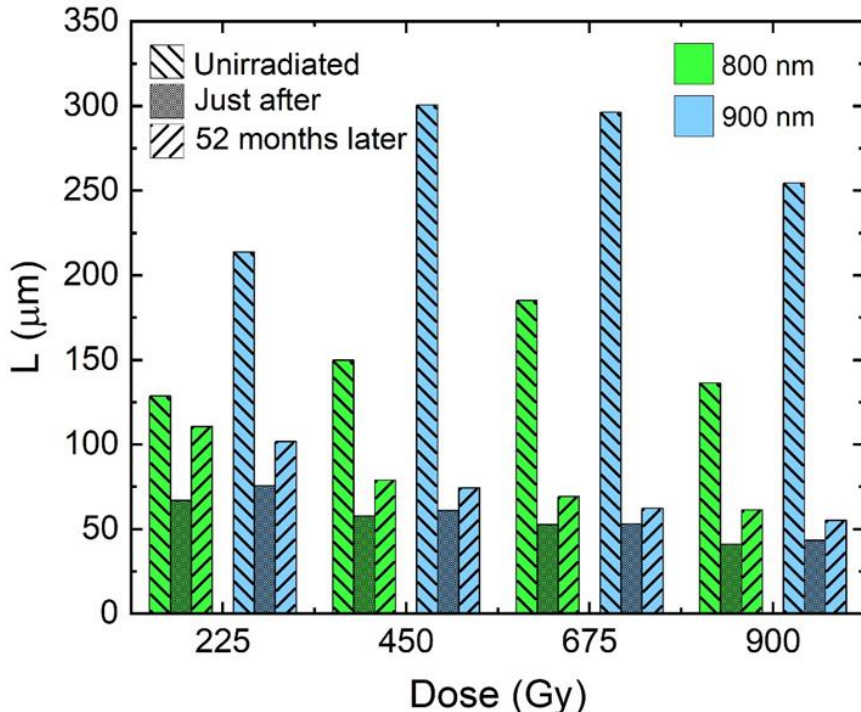


Figure 8. Calculated minority carrier diffusion lengths of electrons from EQE spectrum for different irradiation doses.

Table 5. Percentage of loss and recovery in the diffusion length of electrons calculated at 800 and 900 nm.

Dose (Gy)	Loss in Ln (%)	Recovery in Ln (%)	Loss in Ln (%)	Recovery in Ln (%)
800 nm			900 nm	
225	48	66	65	36
450	61	36	80	21
675	72	30	82	17
900	71	49	83	28

Fig. 9 and 10 illustrate C–V and G/ ω –V characteristics of the cells measured under dark at room temperature, with an AC signal of 100 kHz. For the unirradiated cells, the capacitance exhibits a step-like increase in the forward bias region (0 to \sim 0.5 V), followed by a peak around 1.5 V. In the reverse bias region, the capacitance is dominated by the geometric (depletion) capacitance, as the depletion region width determines the stored charge. Conductance, on the other hand, remains negligible under reverse bias, indicating minimal carrier movement and recombination. The step in the C–V curve, observed between 0 and \sim 0.5 V, corresponds to the transition from the depletion region to the weak injection regime. In this range, the shrinking depletion width causes an increase in capacitance. As the forward bias increases further, a second peak is observed around 1.5 V, marking the transition to the high-injection regime,

where minority carrier injection becomes the dominant factor. This second peak is caused by the diffusion capacitance associated with the storage of injected carriers. Beyond this point, in the very high injection regime, the capacitance decreases due to bulk transport effects. In this regime, carrier saturation and enhanced recombination occur as the injected carriers traverse the bulk of the material, leading to reduced storage capacitance. The G/ω -V curve, in contrast, does not exhibit these distinct peaks or steps. Instead, it shows a gradual increase in conductance as the bias transitions from reverse to forward. This behavior reflects the increasing recombination and carrier transport processes as minority carriers are injected into the device. Subtle features, such as kinks or transitions, may be present in the G/ω -V curve and could be attributed to defect-related processes or trap activation but are generally less pronounced than the peaks in the C-V curve.

After electron irradiation, the C-V and G/ω -V curves display minimal changes in the reverse bias region, indicating that the depletion region remains largely unaffected by radiation-induced defects. However, in the forward bias regime, significant changes are evident. The step and the second peak in the C-V curve are both reduced in magnitude. This reduction is attributed to a decrease in the efficiency of minority carrier injections, caused by enhanced recombination through radiation-induced defects. These defects act as recombination centers, suppressing the diffusion capacitance and limiting carrier storage. In the G/ω -V curve of irradiated cells, the overall conductance is lower in the forward bias region compared to unirradiated cells, consistent with reduced carrier injection and increased recombination. While the kinks or transitions in the G/ω -V curve become less distinct after irradiation, this suggests a suppression of trap-related processes due to the dominance of radiation-induced recombination. The effect of the reduced majority carrier concentration due to compensation by irradiation induced defects could also be one of the main reasons for decrease in capacitance and reduction of conductance in overall behaviors of the cells (Bhat et al., 2014; Oeba et al., 2021; Sathyanarayana Bhat et al., 2015; Yan et al., 2020; Zdravković et al., 2011)

No significant changes are observed in the C-V or G/ω -V behavior of the irradiated cells after a storage period of 52 months. This may be due to the edges of the cells. When cells cut from a full wafer cell, the edges of the cells degraded, and metal residues or metal/Si phases may form around the edge. Which could screen the response of the defects under overall response of the cells. This stability indicates that the radiation-induced defects may remain stable over time under the given conditions, without further evolution or annealing. The persistence of the altered carrier dynamics highlights the long-term impact of electron irradiation on the electrical properties of the solar cells.

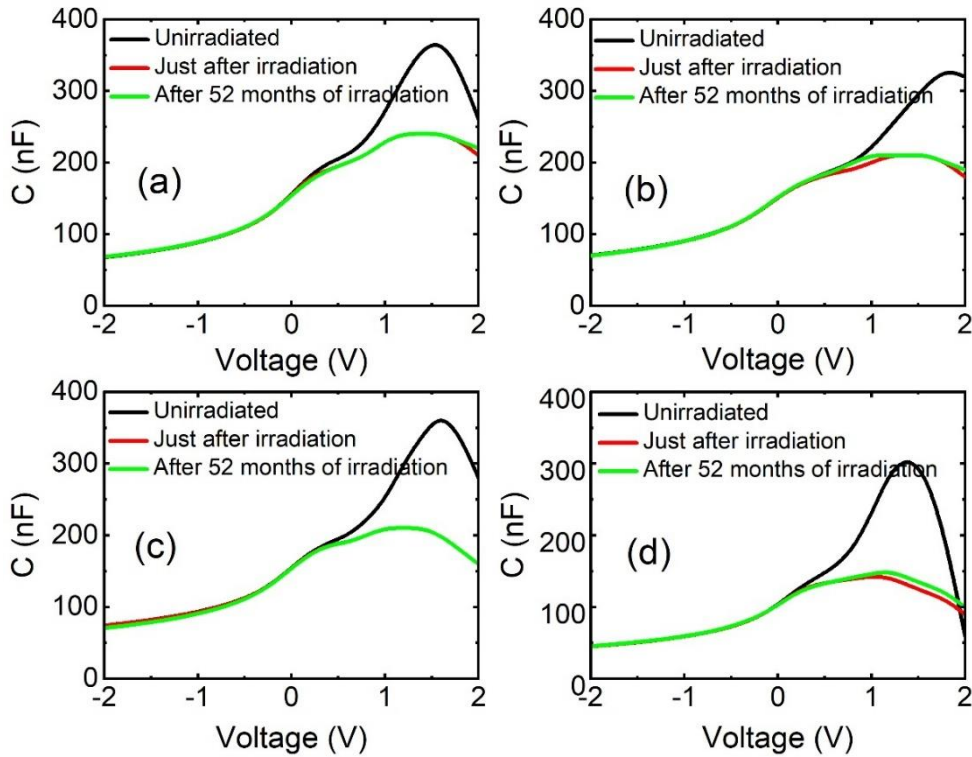


Figure 9. C-V spectrum of the cells measured under dark conditions at room temperature with an applied AC signal of 100 kHz.

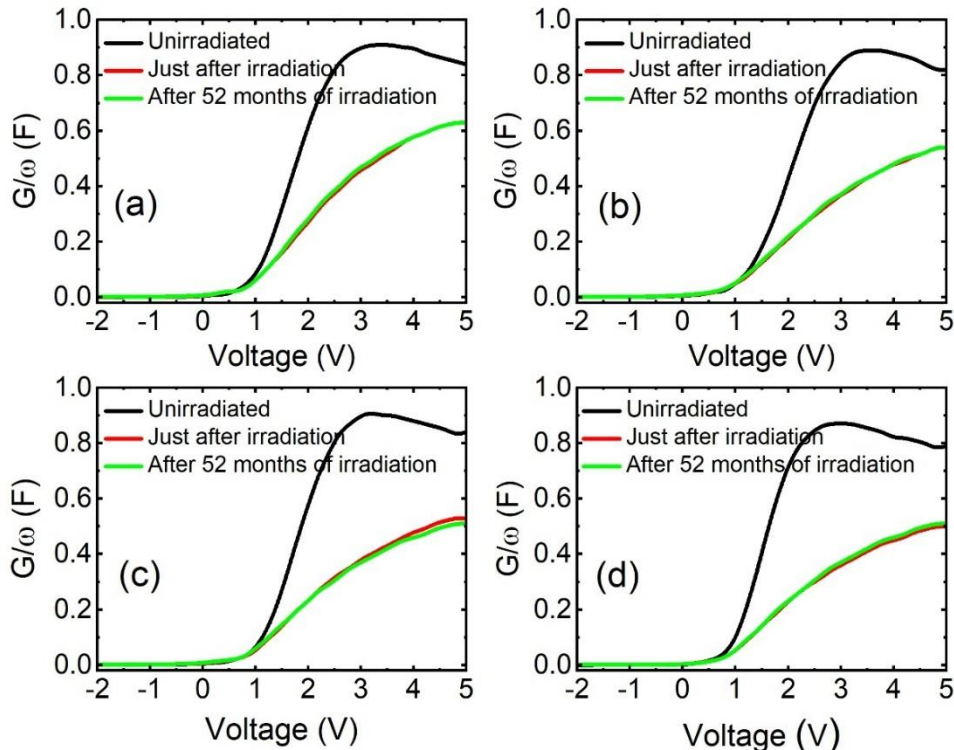


Figure 10. G-V spectrum of the cells measured under dark conditions at room temperature with an applied AC signal of 100 kHz.

4. Conclusions

This study investigated the effects of 8 MeV electron irradiation at different dose levels on c-Si solar cells and their recovery at room temperature after 52 months of irradiation. The experimental results, which compared the different doses, showed a degradation in cell parameters due to radiation-induced defects. As the electron dose level increased from the lowest to the highest dose, there was a significant reduction in efficiency values, with an efficiency loss increasing from 15% to 28%. The primary contribution to the loss of efficiency was due to a reduction in J_{SC} values, compared to moderate loss in V_{OC} . After 52 months of irradiation, a self-healing effect was observed in the devices, particularly as a remarkable recovery in the J_{SC} values. The recovery in current values was consistently verified by illuminated I-V and EQE measurements. Additionally, after 52 months of irradiation, a significant enhancement in the blue response of the cells was observed compared to the unirradiated cells, which was verified by EQE measurements. This enhancement assumed to be due to extra positive charge formation in silicon nitride film as a result oxynitrate formation in ambient atmosphere in time which could be boosted by defects formed by radiation. The observed enhancement in the blue response could pave the way for new passivation approaches for Si solar cells.

Acknowledgements

The author acknowledges the Center for Solar Energy Research and Applications (ODTÜ-GÜNAM) for sample preparation and characterization and the Akdeniz University Nuclear Science Research and Application Center for irradiation facility.

References

- Ali, K., Khan, S.A., MatJafri, M.Z., 2016. Improved radiation resistant properties of electron irradiated c-Si solar cells. *Radiation Physics and Chemistry* 125, 220–226.
<https://doi.org/10.1016/j.radphyschem.2016.04.015>
- Ashry, M., Fares, S., 2003. Diffusion length analysis and measurement in the base region of photodiodes. *Journal of Physics and Chemistry of Solids* 64, 2429–2431.
[https://doi.org/10.1016/S0022-3697\(03\)00285-3](https://doi.org/10.1016/S0022-3697(03)00285-3)
- Babaee, S., Ghozati, S.B., 2017. The study of 1 MeV electron irradiation induced defects in N-type and P-type monocrystalline silicon. *Radiation Physics and Chemistry* 141, 98–102. <https://doi.org/10.1016/j.radphyschem.2017.06.012>
- Basu, P.K., Singh, S.N., Arora, N.K., Chakravarty, B.C., 1994. A New Method of Determination of Minority Carrier Diffusion Length in the Base Region of Silicon Solar Cells. *IEEE Trans Electron Devices* 41, 367–372. <https://doi.org/10.1109/16.275222>

- Bhat, P.S., Rao, A., Krishnan, S., Sanjeev, G., Puthanveettil, S.E., 2014. A study on the variation of c-Si solar cell parameters under 8 MeV electron irradiation. *Solar Energy Materials and Solar Cells* 120, 191–196. <https://doi.org/10.1016/j.solmat.2013.08.043>
- Bodunrin, J.O., Moloi, S.J., 2024. Suppression of irradiation effect on electrical properties of silicon diodes by iron in p-silicon. *Radiation Effects and Defects in Solids* 1–14. <https://doi.org/10.1080/10420150.2024.2382269>
- Bodunrin, J.O., Moloi, S.J., 2022. Current-Voltage Characteristics of 4 MeV Proton-Irradiated Silicon Diodes at Room Temperature. *Silicon* 14, 10237–10244. <https://doi.org/10.1007/s12633-022-01767-8>
- Boztosun, I., Đapo, H., Karakoç, M., Özmen, S.F., Çeçen, Y., Çoban, A., Caner, T., Bayram, E., Saito, T.R., Akdoğan, T., Bozkurt, V., Kuçuk, Y., Kaya, D., Harakeh, M.N., 2015. Photonuclear reactions with zinc: A case for clinical linacs. *Eur Phys J Plus* 130, 185. <https://doi.org/10.1140/epjp/i2015-15185-2>
- Cariou, R., Benick, J., Feldmann, F., Höhn, O., Hauser, H., Beutel, P., Razek, N., Wimplinger, M., Bläsi, B., Lackner, D., Hermle, M., Siefer, G., Glunz, S.W., Bett, A.W., Dimroth, F., 2018. III-V-on-silicon solar cells reaching 33% photoconversion efficiency in two-terminal configuration. *Nat Energy* 3, 326–333. <https://doi.org/10.1038/s41560-018-0125-0>
- Chen, X.C., Li, L., Wang, M.Y., Ren, H., Liu, X.Q., Zeng, G., Yang, G.X., 2024. Carrier-induced formation of electrically active boron-interstitial clusters in irradiated boron-doped silicon. *J Appl Phys* 135, 055101. <https://doi.org/10.1063/5.0172704>
- Danilchenko, B., Budnyk, A., Shpinar, L., Poplavskyy, D., Zelensky, S.E., Barnham, K.W.J., Ekins-Daukes, N.J., 2008. 1 MeV electron irradiation influence on GaAs solar cell performance. *Solar Energy Materials and Solar Cells* 92, 1336–1340. <https://doi.org/10.1016/j.solmat.2008.05.006>
- Es, F., Kulakci, M., Turan, R., 2016. An Alternative Metal-Assisted Etching Route for Texturing Silicon Wafers for Solar Cell Applications. *IEEE J Photovolt* 6, 440–446. <https://doi.org/10.1109/JPHOTOV.2016.2520207>
- Essig, S., Allebé, C., Remo, T., Geisz, J.F., Steiner, M.A., Horowitz, K., Barraud, L., Ward, J.S., Schnabel, M., Descoedres, A., Young, D.L., Woodhouse, M., Despeisse, M., Ballif, C., Tamboli, A., 2017. Raising the one-sun conversion efficiency of III-V/Si solar cells to 32.8% for two junctions and 35.9% for three junctions. *Nat Energy* 2, 17144. <https://doi.org/10.1038/nenergy.2017.144>
- Essig, S., Steiner, M.A., Allebé, C., Geisz, J.F., Paviet-Salomon, B., Ward, S., Descoedres, A., LaSalvia, V., Barraud, L., Badel, N., Faes, A., Levrat, J., Despeisse, M., Ballif, C., Stradins, P., Young, D.L., 2016. Realization of GaInP/Si Dual-Junction Solar Cells with 29.8% 1-Sun Efficiency. *IEEE J Photovolt* 6, 1012–1019. <https://doi.org/10.1109/JPHOTOV.2016.2549746>
- Feick, H., 1997. Radiation tolerance of silicon particle detectors for high energy physics. Hamburg.

- 1 Feklisova, O. V., Yarykin, N.A., Weber, J., 2013. Annealing kinetics of boron-containing
2 centers in electron-irradiated silicon. Semiconductors 47, 228–231.
3 https://doi.org/10.1134/S1063782613020085
- 4 Giesecke, J.A., Michl, B., Schindler, F., Schubert, M.C., Warta, W., 2011. Minority carrier
5 lifetime of silicon solar cells from quasi-steady-state photoluminescence. Solar Energy
6 Materials and Solar Cells 95, 1979–1982. https://doi.org/10.1016/j.solmat.2011.02.023
7
- 8 Green, M.A., 2016. Commercial progress and challenges for photovoltaics. Nat Energy 1,
9 15015. https://doi.org/10.1038/nenergy.2015.15
- 10 Hamache, A., Sengouga, N., Meftah, A., Henini, M., 2016. Modeling the effect of 1 MeV
11 electron irradiation on the performance of n+-p-p+ silicon space solar cells. Radiation
12 Physics and Chemistry 123, 103–108.
13 https://doi.org/10.1016/j.radphyschem.2016.02.025
- 14 Hisamatsu, T., Kawasaki, O., Matsuda, S., Nakao, T., Wakow, Y., 1998. Radiation
15 degradation of large fluence irradiated space silicon solar cells. Solar Energy Materials
16 and Solar Cells 50, 331–338. https://doi.org/10.1016/S0927-0248(97)00163-3
- 17 Honsberg, C., Bowden, S., 2019. Generation Rate [WWW Document]. URL
18 https://www.pveducation.org/pvcdrom/pn-junctions/generation-rate (accessed 1.19.25).
- 19 Horiuchi, N., Nozaki, T., Chiba, A., 2000. Improvement in electrical performance of
20 radiation-damaged silicon solar cells by annealing. Nucl Instrum Methods Phys Res A
21 443, 186–193. https://doi.org/10.1016/S0168-9002(99)01013-X
- 22 Imaizumi, M., Taylor, S.J., Yamaguchi, M., Ito, T., Hisamatsu, T., Matsuda, S., 1999.
23 Analysis of structure change of Si solar cells irradiated with high fluence electrons 85,
24 1916–1920. https://doi.org/10.1063/1.369184
- 25 Jasenek, A., Rau, U., 2001. Defect generation in Cu(In,Ga)Se₂ heterojunction solar cells by
26 high-energy electron and proton irradiation. J Appl Phys 90, 650–658.
27 https://doi.org/10.1063/1.1379348
- 28 Junga, F.A., Enslow, G.M., 1959. Radiation Effects in Silicon Solar Cells. IRE Transactions
29 on Nuclear Science 6, 49–53. https://doi.org/10.1109/TNS2.1959.4315679
- 30 Kabaçelik, İ., 2023. Investigation of the Effect of Successive Low-Dose γ -Rays on c-Si Solar
31 Cell. Gazi Üniversitesi Fen Bilimleri Dergisi Part C: Tasarım ve Teknoloji 11, 582–591.
32 https://doi.org/10.29109/gujsc.1199922
- 33 Kabacelik, I., Kutaruk, H., Yaltkaya, S., Sahin, R., 2017. γ irradiation induced effects on the
34 TCO thin films. Radiation Physics and Chemistry 134, 89–92.
35 https://doi.org/10.1016/j.radphyschem.2017.01.042
- 36 Kawakita, S., Imaizumi, M., Yamaguchi, M., Kushiya, K., Ohshima, T., Itoh, H., Matsuda, S.,
37 2002. Annealing enhancement effect by light illumination on proton irradiated
38 Cu(In,Ga)Se₂ thin-film solar cells. Jpn J Appl Phys 41, L797–L799.
39 https://doi.org/10.1143/jjap.41.1797
- 40 Khan, A., Yamaguchi, M., Ohshita, Y., Dharmaraso, N., Araki, K., Khanh, V.T., Itoh, H.,
41 Ohshima, T., Imaizumi, M., Matsuda, S., 2003. Strategies for improving radiation
42

tolerance of Si space solar cells. *Solar Energy Materials & Solar Cells* 75, 271–276.
[https://doi.org/10.1016/S0927-0248\(02\)00169-1](https://doi.org/10.1016/S0927-0248(02)00169-1)

Krishnan, S., Sanjeev, G., Pattabi, M., 2007. 8 MeV electron irradiation effects in silicon photo-detectors. *Nucl Instrum Methods Phys Res B* 264, 79–82.
<https://doi.org/10.1016/j.nimb.2007.08.004>

Krishnan, S., Sanjeev, G., Pattabi, M., Mathew, X., 2009. Effect of electron irradiation on the properties of CdTe/CdS solar cells. *Solar Energy Materials and Solar Cells* 93, 2–5.
<https://doi.org/10.1016/j.solmat.2007.12.002>

Kuendig, J., Goetz, M., Shah, A., Gerlach, L., Fernandez, E., 2003. Thin film silicon solar cells for space applications: Study of proton irradiation and thermal annealing effects on the characteristics of solar cells and individual layers. *Solar Energy Materials and Solar Cells* 79, 425–438. [https://doi.org/10.1016/S0927-0248\(02\)00486-5](https://doi.org/10.1016/S0927-0248(02)00486-5)

Kulakci, M., Es, F., Ozdemir, B., Unalan, H.E., Turan, R., 2013. Application of si nanowires fabricated by metal-assisted etching to crystalline si solar cells. *IEEE J Photovolt* 3, 548–553. <https://doi.org/10.1109/JPHOTOV.2012.2228300>

Lang, F., Nickel, N.H., Bundesmann, J., Seidel, S., Denker, A., Albrecht, S., Brus, V. V., Rappich, J., Rech, B., Landi, G., Neitzert, H.C., 2016. Radiation Hardness and Self-Healing of Perovskite Solar Cells. *Advanced Materials* 28, 8726–8731.
<https://doi.org/10.1002/adma.201603326>

Leguijt, C., Lislegen, P., Eikelboom, J.A., Weeber, A.W., Schuurmans, F.M., Sinke, W.C., Alkemade, P.F.A., Sarro, P.M., Marte, C.H.M., Verhoef, L.A., 1996. Low temperature surface passivation for silicon solar cells. *Solar Energy Materials and Solar Cells* 40, 297–345. [https://doi.org/10.1016/0927-0248\(95\)00155-7](https://doi.org/10.1016/0927-0248(95)00155-7)

Lelièvre, J.-F, Fourmond, E., Kaminski, A., Palais, Olivier, Balltaud, D., Lemiti, M., Lelièvre, J-F, Palais, O, 2009. Study of the composition of hydrogenated silicon nitride SiNx:H for efficient surface and bulk passivation of silicon. *Solar Energy Materials and Solar Cells* 93, 1281–1289. <https://doi.org/10.1016/j.solmat.2009.01.023>

Li, J., Aierken, A., Liu, Y., Zhuang, Y., Yang, X., Mo, J.H., Fan, R.K., Chen, Q.Y., Zhang, S.Y., Huang, Y.M., Zhang, Q., 2021. A Brief Review of High Efficiency III-V Solar Cells for Space Application. *Front Phys* 8, 631925.
<https://doi.org/10.3389/fphy.2020.631925>

Li, P., Dong, H., Lan, J., Bai, Y., He, C., Ma, L., Li, Y., Liu, J., 2022. Tolerance of Perovskite Solar Cells under Proton and Electron Irradiation. *Materials* 15, 1393.
<https://doi.org/10.3390/ma15041393>

Liao, C., Fretwurst, E., Garutti, E., Schwandt, J., Makarenko, L., Pintilie, I., Filip, L.D., Himmerlich, A., Moll, M., Gurimskaya, Y., Li, Z., 2023. Investigation of the Boron removal effect induced by 5.5MeV electrons on highly doped EPI- and Cz-silicon. *Nucl Instrum Methods Phys Res A* 1056, 168559. <https://doi.org/10.1016/j.nima.2023.168559>

Liao, C., Fretwurst, E., Garutti, E., Schwandt, J., Pintilie, I., Nitescu, A., Himmerlich, A., Moll, M., Gurimskaya, Y., Li, Z., 2024. Investigation of high resistivity p-type FZ

silicon diodes after 60Co γ -irradiation. Nucl Instrum Methods Phys Res A 1061, 169103.
<https://doi.org/10.1016/j.nima.2024.169103>

Luft, W., 1964. Effects of Electron Irradiation on N on P Silicon Solar Cells. IEEE Transactions on Aerospace 2, 747–758. <https://doi.org/10.1109/TA.1964.4319662>

Matsuura, H., Iwata, H., Kagamihara, S., Ishihara, R., Komeda, M., Imai, H., Kikuta, M., Inoue, Y., Hisamatsu, T., Kawakita, S., Ohshima, T., Itoh, H., 2006. Si substrate suitable for radiation-resistant space solar cells. Jpn J Appl Phys 45, 2648–2655.
<https://doi.org/10.1143/JJAP.45.2648>

Medjoubi, K., Lefèvre, J., Vauche, L., Veinberg-Vidal, E., Jany, C., Rostaing, C., Amalbert, V., Chabuel, F., Boizot, B., Cariou, R., 2021. Electrons irradiation of III-V//Si solar cells for NIRT conditions. Solar Energy Materials and Solar Cells 223, 110975.
<https://doi.org/10.1016/j.solmat.2021.110975>

Mizuno, H., Makita, K., Sai, H., Mochizuki, T., Matsui, T., Takato, H., Müller, R., Lackner, D., Dimroth, F., Sugaya, T., 2022. Integration of Si Heterojunction Solar Cells with III-V Solar Cells by the Pd Nanoparticle Array-Mediated “Smart Stack” Approach. ACS Appl Mater Interfaces 14, 11322–11329. <https://doi.org/10.1021/acsami.1c22458>

Moll, M., 1999. Radiation damage in silicon particle detectors. Hamburg.

Morita, Y., Ohshima, T., Nashiyama, I., Yamamoto, Y., Kawasaki, O., Matsuda, S., 1997. Anomalous degradation in silicon solar cells subjected to high-fluence proton and electron irradiations. J Appl Phys 81, 6491–6493. <https://doi.org/10.1063/1.364437>

Nikolić, D., Stanković, K., Timotijević, L., Rajović, Z., Vujisić, M., 2013. Comparative study of gamma radiation effects on solar cells, photodiodes, and phototransistors. International Journal of Photoenergy 2013, 843174. <https://doi.org/10.1155/2013/843174>

Nikolić, D., Vasić-Milovanović, A., Obrenović, M., Dolićanin, E., 2015. Effects of successive gamma and neutron irradiation on solar cells. Journal of Optoelectronics and Advanced Materials 17, 351–356.

Oeba, D.A., Bodunrin, J.O., Moloi, S.J., 2024. Enhancing radiation-hardness of Si-based diodes: An investigation of Al-doping effects in Si using I–V measurements. Radiation Physics and Chemistry 223, 111873. <https://doi.org/10.1016/j.radphyschem.2024.111873>

Oeba, D.A., Bodunrin, J.O., Moloi, S.J., 2021. Electrical properties of 3 MeV proton irradiated silicon Schottky diodes. Physica B Condens Matter 610, 412786.
<https://doi.org/10.1016/j.physb.2020.412786>

Onoda, S., Hirao, T., Laird, J.S., Mori, H., Okamoto, T., Koizumi, Y., Itoh, H., 2002. Spectral response of a gamma and electron irradiated pin photodiode. IEEE Trans Nucl Sci 49, 1446–1449. <https://doi.org/10.1109/TNS.2002.1039681>

Pellegrino, C., Gagliardi, A., Zimmermann, C.G., 2019. Difference in space-charge recombination of proton and electron irradiated GaAs solar cells. Progress in Photovoltaics: Research and Applications 27, 379–390. <https://doi.org/10.1002/pip.3100>

Radu, R., Fretwurst, E., Klanner, R., Lindstroem, G., Pintilie, I., 2013. Radiation damage in n-type silicon diodes after electron irradiation with energies between 1.5 MeV and 15

1 MeV. Nucl Instrum Methods Phys Res A 730, 84–90.
2 https://doi.org/10.1016/j.nima.2013.04.080

3 Raider, S.I., Flitsch, R., Aboaf, J.A., Pliskin, W.A., 1976. Surface Oxidation of Silicon
4 Nitride Films. J Electrochem Soc 123, 560–565. https://doi.org/10.1149/1.2132877

5 Raya-Armenta, J.M., Bazmohammadi, N., Vasquez, J.C., Guerrero, J.M., 2021. A short
6 review of radiation-induced degradation of III–V photovoltaic cells for space
7 applications. Solar Energy Materials and Solar Cells 233, 111379.
8 https://doi.org/10.1016/j.solmat.2021.111379

9 Robertson, J., 1993. Electronic Structure of Defects in Amorphous Silicon Nitride. MRS
10 Online Proceedings Library 284, 65–76. https://doi.org/10.1557/PROC-284-65

11 Saad, A.M., 2002. Effect of cobalt 60 and 1 MeV electron irradiation on silicon
12 photodiodes/solar cells. Can J Phys 80, 1591–1599. https://doi.org/10.1139/p02-037

13 Sahin, R., Kabacelik, I., 2018. Effects of ionizing radiation on the properties of mono-
14 crystalline Si solar cells. Radiation Physics and Chemistry 150, 90–94.
15 https://doi.org/10.1016/j.radphyschem.2018.04.033

16 Sathyanarayana Bhat, P., Rao, A., Sanjeev, G., Usha, G., Priya, G.K., Sankaran, M.,
17 Puthanveettil, S.E., 2015. Capacitance and conductance studies on silicon solar cells
18 subjected to 8MeV electron irradiations. Radiation Physics and Chemistry 111, 28–35.
19 https://doi.org/10.1016/j.radphyschem.2015.02.010

20 Sato, S. ichiro, Miyamoto, H., Imaizumi, M., Shimazaki, K., Morioka, C., Kawano, K.,
21 Ohshima, T., 2009. Degradation modeling of InGaP/GaAs/Ge triple-junction solar cells
22 irradiated with various-energy protons. Solar Energy Materials and Solar Cells 93, 768–
23 773. https://doi.org/10.1016/j.solmat.2008.09.044

24 Schmidt, J., Aberle, A.G., 1999. Carrier recombination at silicon-silicon nitride interfaces
25 fabricated by plasma-enhanced chemical vapor deposition. J Appl Phys 85, 3626–3633.
26 https://doi.org/10.1063/1.369725

27 Schmidt, J., Berge, C., Aberle, A.G., 1998. Injection level dependence of the defect-related
28 carrier lifetime in light-degraded boron-doped Czochralski silicon. Appl Phys Lett 73,
29 2167–2169. https://doi.org/10.1063/1.122411

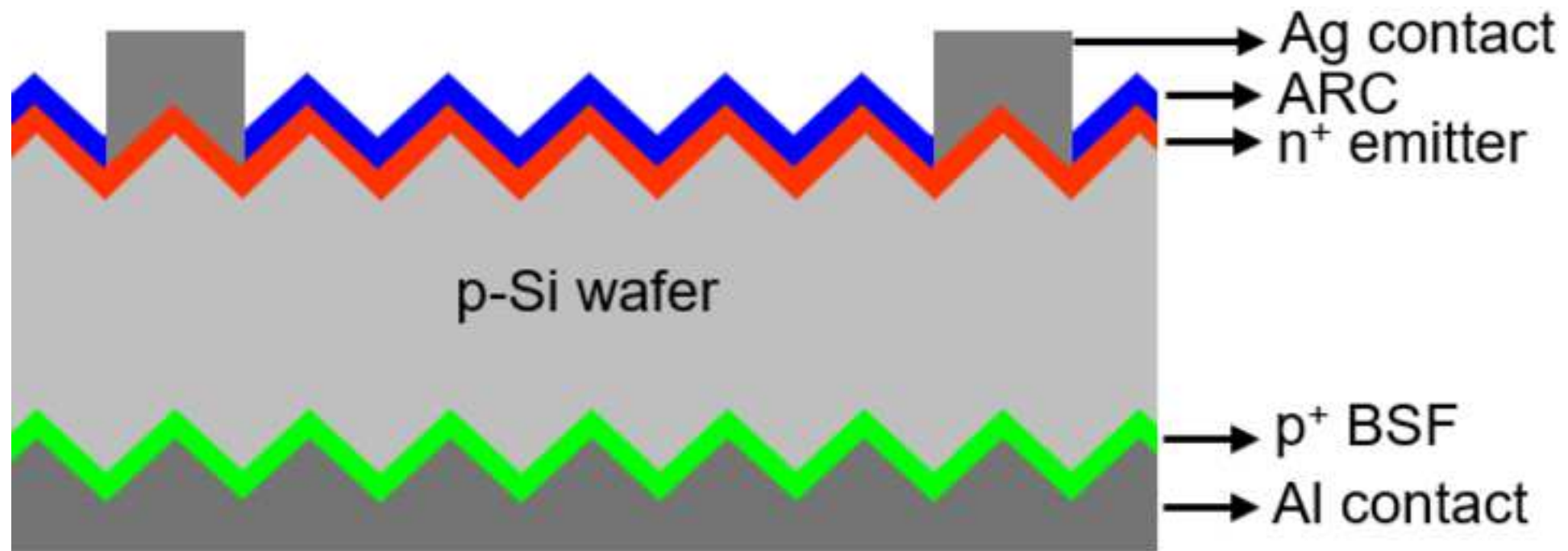
30 Schnabel, M., Schulte-Huxel, H., Rienäcker, M., Warren, E.L., Ndione, P.F., Nemeth, B.,
31 Klein, T.R., Van Hest, M.F.A.M., Geisz, J.F., Peibst, R., Stradins, P., Tamboli, A.C.,
32 2020. Three-terminal III-V/Si tandem solar cells enabled by a transparent conductive
33 adhesive. Sustain Energy Fuels 4, 549–558. https://doi.org/10.1039/c9se00893d

34 Schygulla, P., Müller, R., Lackner, D., Höhn, O., Hauser, H., Bläsi, B., Predan, F., Benick, J.,
35 Hermle, M., Glunz, S.W., Dimroth, F., 2022. Two-terminal III–V/Si triple-junction solar
36 cell with power conversion efficiency of 35.9 % at AM1.5g. Progress in Photovoltaics:
37 Research and Applications 30, 869–879. https://doi.org/10.1002/pip.3503

38 Sharma, D., Mehra, R., Raj, B., 2022. Methods for Integration of III-V Compound and Silicon
39 Multijunction for High Efficiency Solar Cell Design. Silicon 14, 9797–9804.
40 https://doi.org/10.1007/s12633-022-01691-x

- Sharma, V., Tracy, C., Schroder, D., Flores, M., Dauksher, B., Bowden, S., 2013. Study and manipulation of charges present in silicon nitride films, in: Conference Record of the IEEE Photovoltaic Specialists Conference. Institute of Electrical and Electronics Engineers Inc., pp. 1288–1293. <https://doi.org/10.1109/PVSC.2013.6744377>
- Shen, X.B., Aierken, A., Heini, M., Mo, J.H., Lei, Q.Q., Zhao, X.F., Sailai, M., Xu, Y., Tan, M., Wu, Y.Y., Lu, S.L., Li, Y.D., Guo, Q., 2019. Degradation analysis of 1 MeV electron and 3 MeV proton irradiated InGaAs single junction solar cell. *AIP Adv* 9, 075205. <https://doi.org/10.1063/1.5094472>
- Srour, J.R., Marshall, C.J., Marshall, P.W., 2003. Review of displacement damage effects in silicon devices. *IEEE Trans Nucl Sci* 50, 653–670. <https://doi.org/10.1109/TNS.2003.813197>
- Srour, J.R., Palko, J.W., 2013. Displacement damage effects in irradiated semiconductor devices. *IEEE Trans Nucl Sci* 60, 1740–1766. <https://doi.org/10.1109/TNS.2013.2261316>
- Summers, G.P., Burke, E.A., Xapsos, M.A., 1995. Displacement damage analogs to ionizing radiation effects. *Radiat Meas* 24, 1–8. [https://doi.org/10.1016/1350-4487\(94\)00093-G](https://doi.org/10.1016/1350-4487(94)00093-G)
- Svensson, B.G., Jagadish, C., Hallé, A., Lalita, J., 1997. Generation of vacancy-type point defects in single collision cascades during swift-ion bombardment of silicon. *Phys Rev B* 55, 10498. <https://doi.org/10.1103/PhysRevB.55.10498>
- Taylor, S.J., Yamaguchi, M., Yang, M.J., Imaizumi, M., Matsuda, S., Kawasaki, O., Hisamatsu, T., 1997. Type conversion in irradiated silicon diodes. *Appl Phys Lett* 70, 2165–2167. <https://doi.org/10.1063/1.118946>
- Tobnaghi, D.M., Rahnamaei, A., Vajdi, M., 2014. Experimental Study of Gamma Radiation Effects on the Electrical Characteristics of Silicon Solar Cells. *Int. J. Electrochem. Sci.* 9, 2824–2831.
- Verduci, R., Romano, V., Brunetti, G., Yaghoobi Nia, N., Di Carlo, A., D'Angelo, G., Ciminelli, C., 2022. Solar Energy in Space Applications: Review and Technology Perspectives. *Adv Energy Mater* 12, 2200125. <https://doi.org/10.1002/aenm.202200125>
- Weiss, C., Park, S., Lefèvre, J., Boizot, B., Mohr, C., Cavani, O., Picard, S., Kurstjens, R., Niewelt, T., Janz, S., 2020. Electron and proton irradiation effect on the minority carrier lifetime in SiC passivated p-doped Ge wafers for space photovoltaics. *Solar Energy Materials and Solar Cells* 209, 110430. <https://doi.org/10.1016/j.solmat.2020.110430>
- Wolf, M., Noel, G.T., Stirn, R.J., 1977. Investigation of the Double Exponential in the Current-Voltage Characteristics of Silicon Solar cells. *EEE Transactions on Electron Devices* 24, 419–428. <https://doi.org/10.1109/T-ED.1977.18750>
- Wunstorf, R., Bugg, W.M., Walter, J., Garber, F.W., Larson, D., 1996. Investigations of donor and acceptor removal and long term annealing in silicon with different boron/phosphorus ratios. *Nuclear Instruments and Methods in Physics Research A* 377, 228–233. [https://doi.org/10.1016/0168-9002\(96\)00217-3](https://doi.org/10.1016/0168-9002(96)00217-3)

- Yamaguchi, M., 2001. Radiation-resistant solar cells for space use. *Solar Energy Materials and Solar Cells* 68, 31–53. [https://doi.org/10.1016/S0927-0248\(00\)00344-5](https://doi.org/10.1016/S0927-0248(00)00344-5)
- Yamaguchi, M., Khan, A., Taylor, S.J., Ando, K., Yamaguchi, T., Matsuda, S., Aburaya, T., 1999. Deep level analysis of radiation-induced defects in Si crystals and solar cells. *J Appl Phys* 86, 217–223. <https://doi.org/10.1063/1.370698>
- Yamaguchi, M., Taylor, S.J., Matsuda, S., Kawasaki, O., Ando, K., 1996. Analysis of damage to silicon solar cells by high fluence electron irradiation, in: Conference Record of the IEEE Photovoltaic Specialists Conference. IEEE, pp. 167–170. <https://doi.org/10.1109/pvsc.1996.563973>
- Yan, G., Wang, J. ling, Liu, J., Liu, Y. yu, Wu, R., Wang, R., 2020. Electroluminescence analysis of VOC degradation of individual subcell in GaInP/GaAs/Ge space solar cells irradiated by 1.0 MeV electrons. *J Lumin* 219, 116905. <https://doi.org/10.1016/j.jlumin.2019.116905>
- Yang, J., Bao, Q., Shen, L., Ding, L., 2020. Potential applications for perovskite solar cells in space. *Nano Energy* 76, 105019. <https://doi.org/10.1016/j.nanoen.2020.105019>
- Yang, S.-S., Gao, X., Wang, Y.-F., Feng, Z.-Z., 2011. Displacement Damage Characterization of Electron Radiation in Triple-Junction GaAs Solar Cells. *J Spacecr Rockets* 48, 23–26. <https://doi.org/10.2514/1.48873>
- Yu, S., Rabelo, M., Yi, J., 2022. A Brief Review on III-V/Si Tandem Solar Cells. *Transactions on Electrical and Electronic Materials* 23, 327–336. <https://doi.org/10.1007/s42341-022-00398-5>
- Zdravković, M.R., Vasić, A.I., Radosavljević, R.L., Vujišić, M.L., Osmokrović, P. V., 2011. Influence of radiation on the properties of solar cells. *Nuclear Technology and Radiation Protection* 26, 158–163. <https://doi.org/10.2298/NTRP1102158Z>
- Zh Karazhanov, S., 2000. Effect of radiation-induced defects on silicon solar cells. *J Appl Phys* 88, 3941–3947. <https://doi.org/10.1063/1.1290453>
- Zhang, Y., Qi, C., Wang, T., Ma, G., Tsai, H.S., Liu, C., Zhou, J., Wei, Y., Li, H., Xiao, L., Ma, Y., Wang, D., Tang, C., Li, J., Wu, Z., Huo, M., 2020. Electron Irradiation Effects and Defects Analysis of the Inverted Metamorphic Four-Junction Solar Cells. *IEEE J Photovolt* 10, 1712–1720. <https://doi.org/10.1109/JPHOTOV.2020.3025442>
- Zhang, Y., Zhang, H., Yu, B., Wang, W., Hou, R., Chen, B., Xu, Q., Zhou, Y., Qin, G., 2014. Gamma-ray irradiation hardness of arrayed silicon microhole-based radial p-n junction solar cells. *J Phys D Appl Phys* 47, 065101. <https://doi.org/10.1088/0022-3727/47/6/065101>



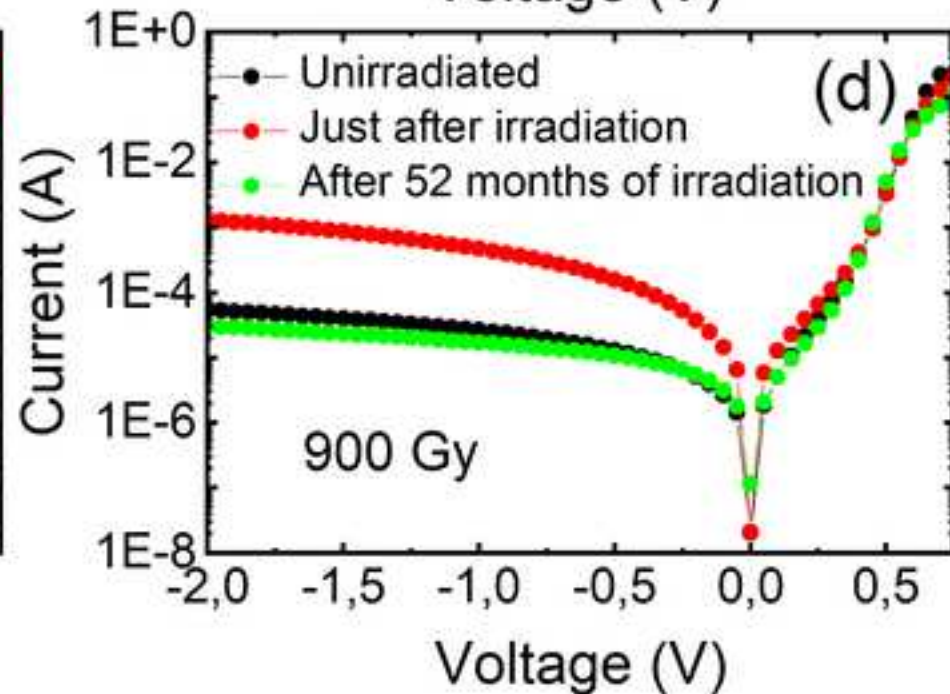
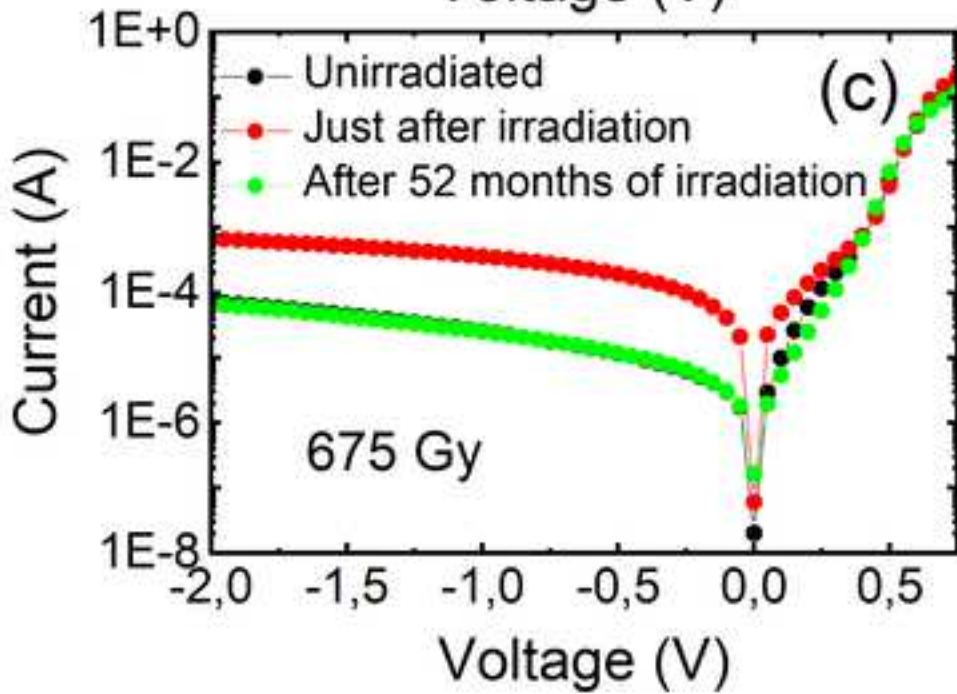
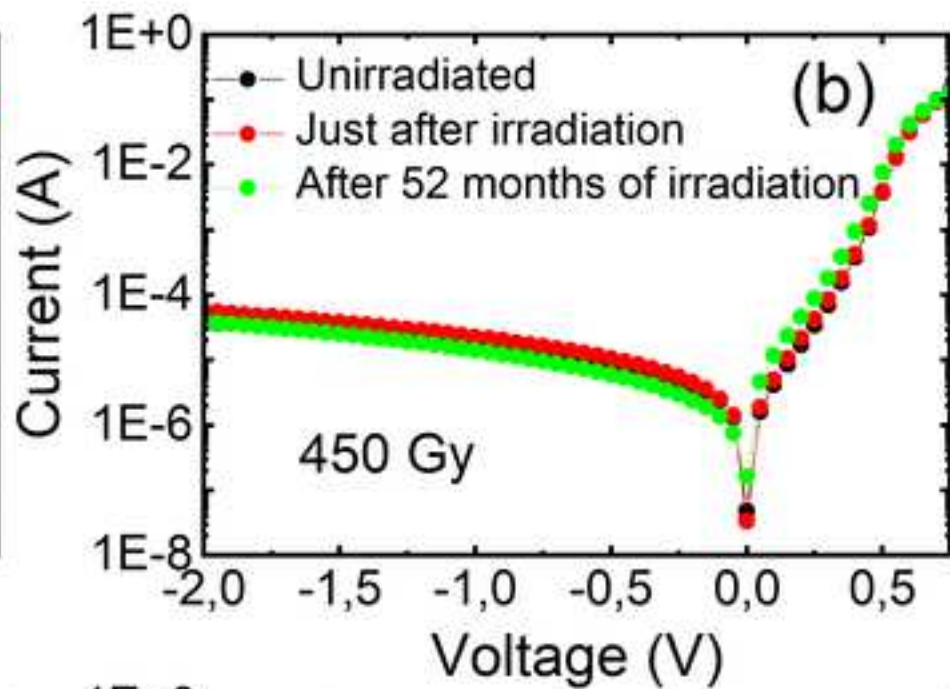
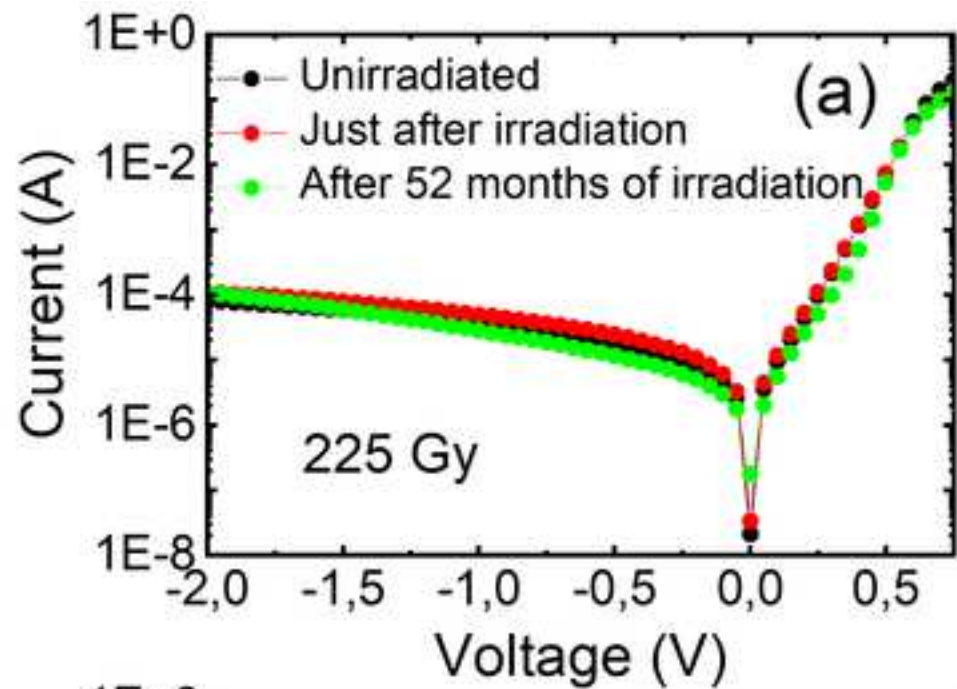


Figure 3

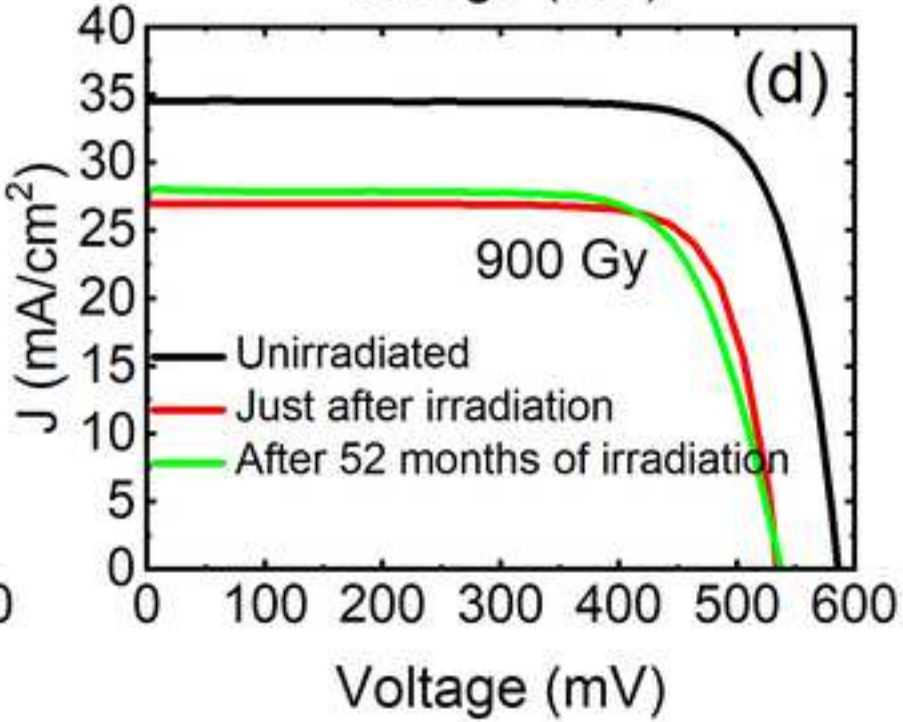
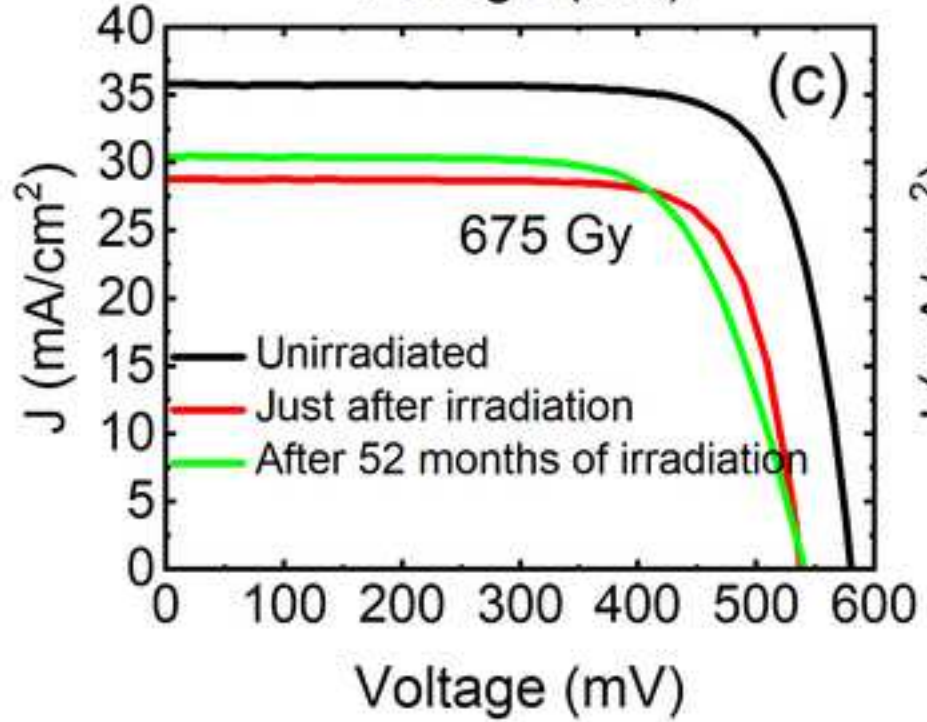
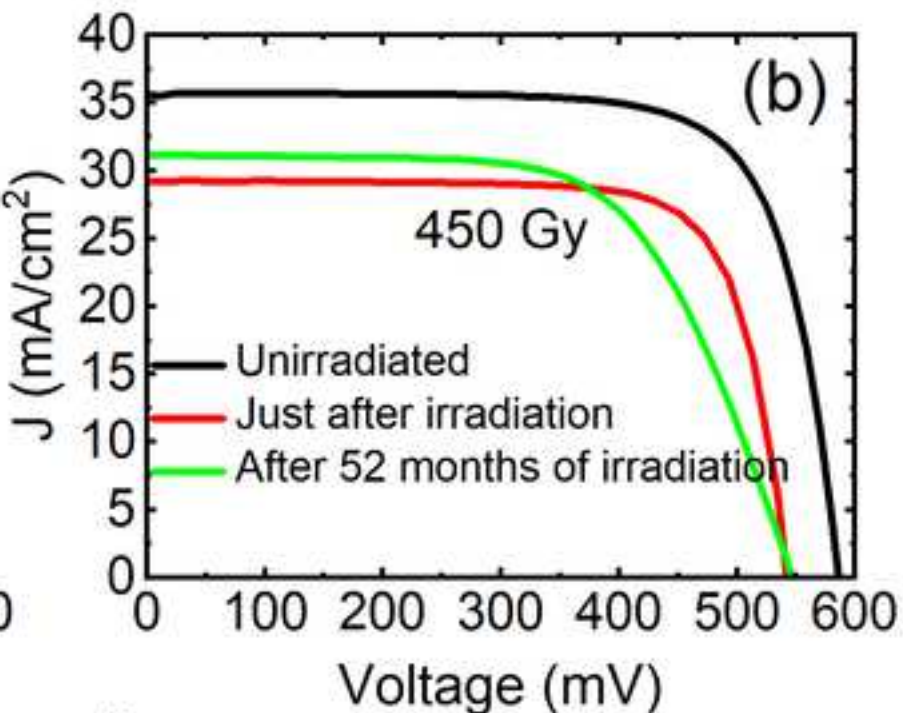
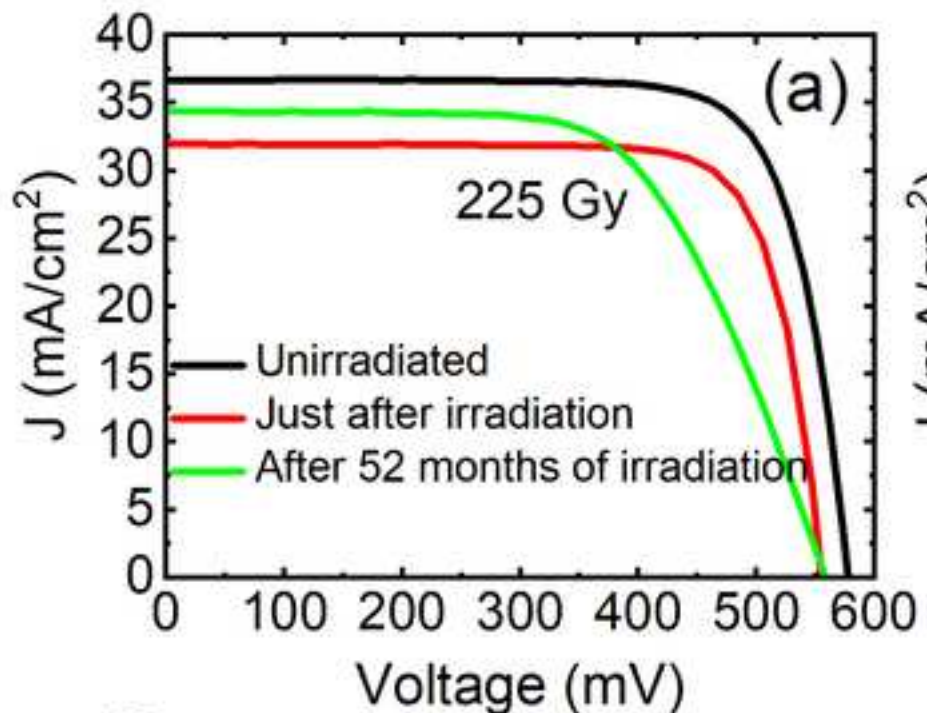
[Click here to access/download;Figure;Figure 3.jpg](#)

Figure 4a

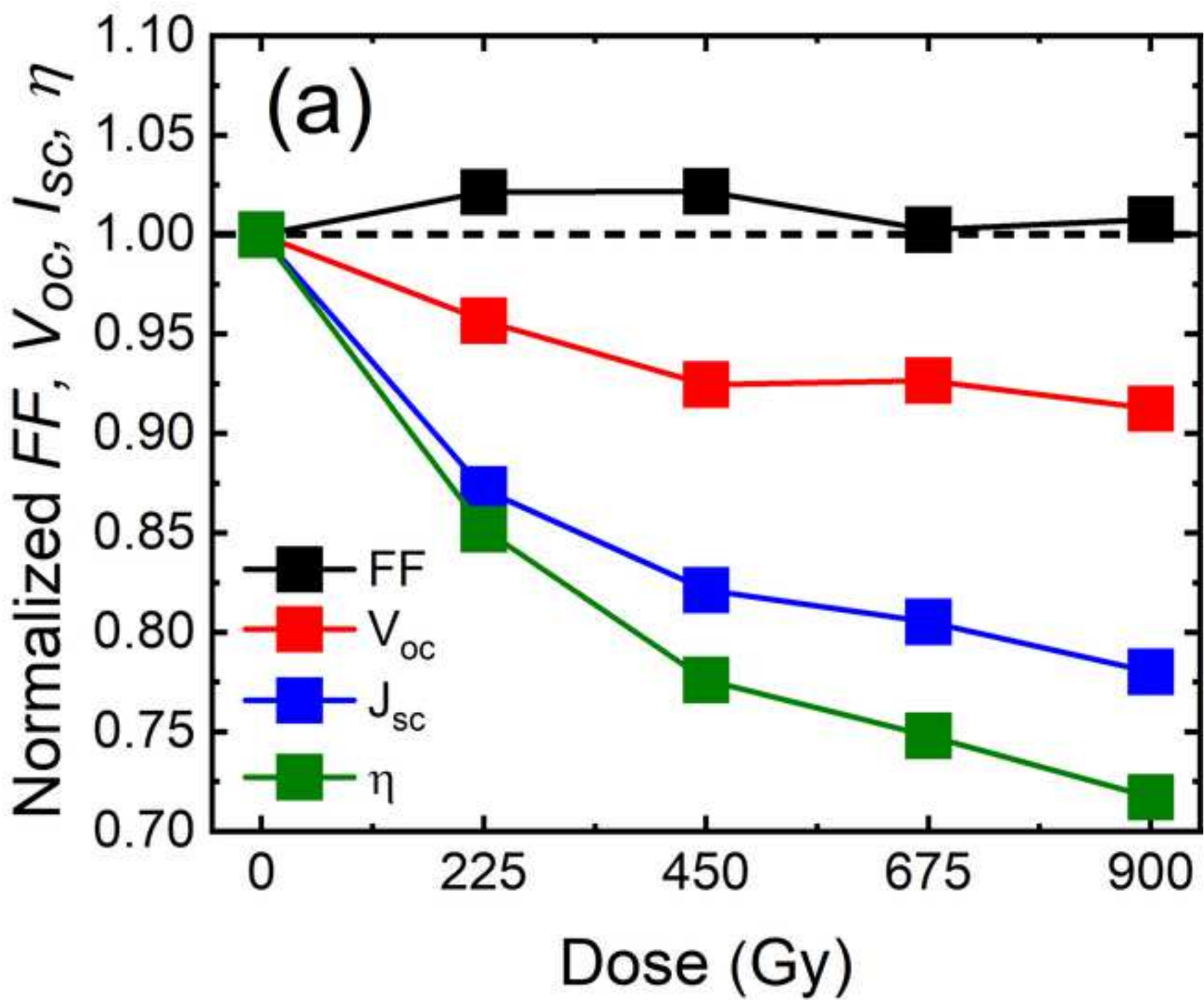
[Click here to access/download;Figure;Figure 4a.jpg](#)

Figure 4b

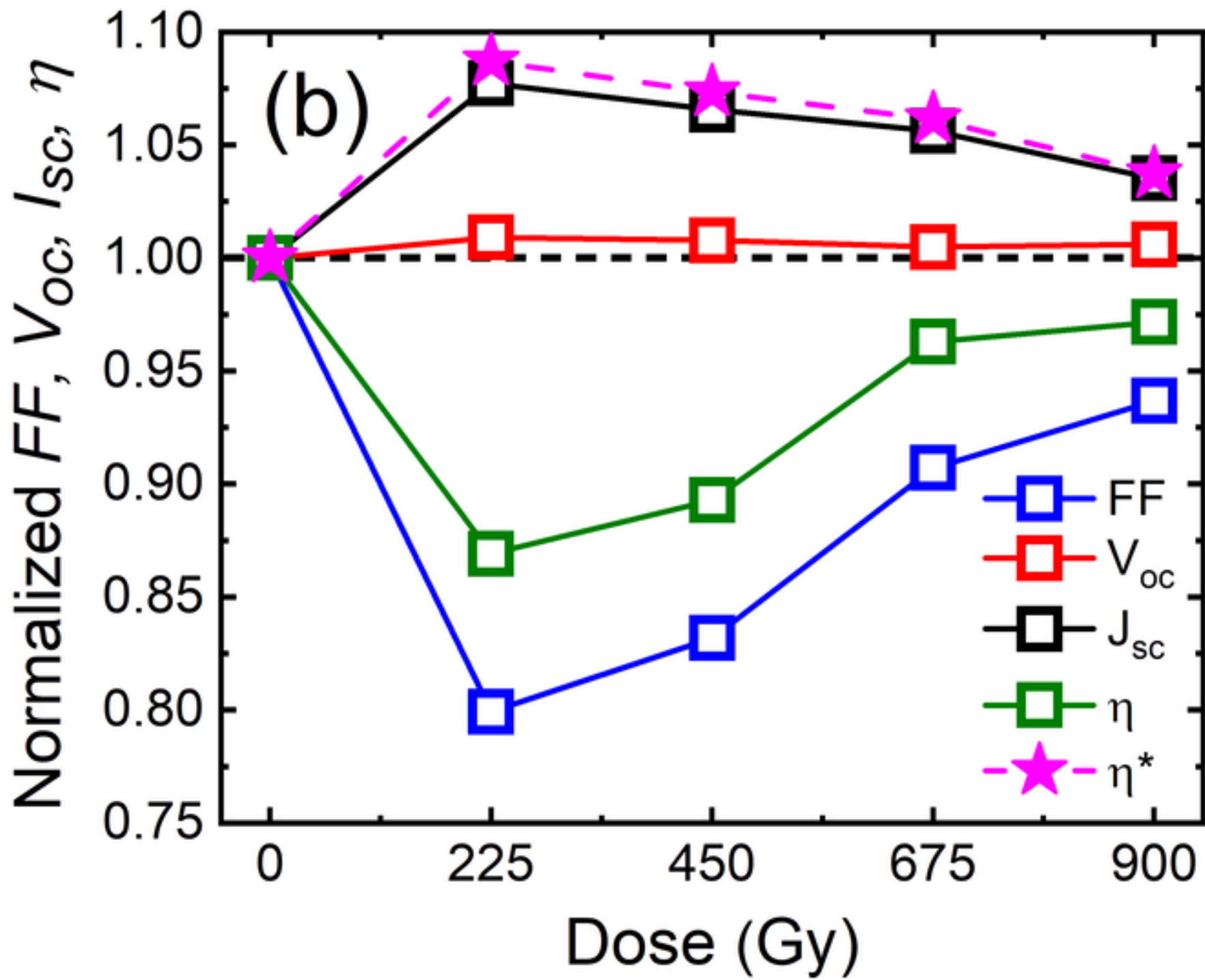
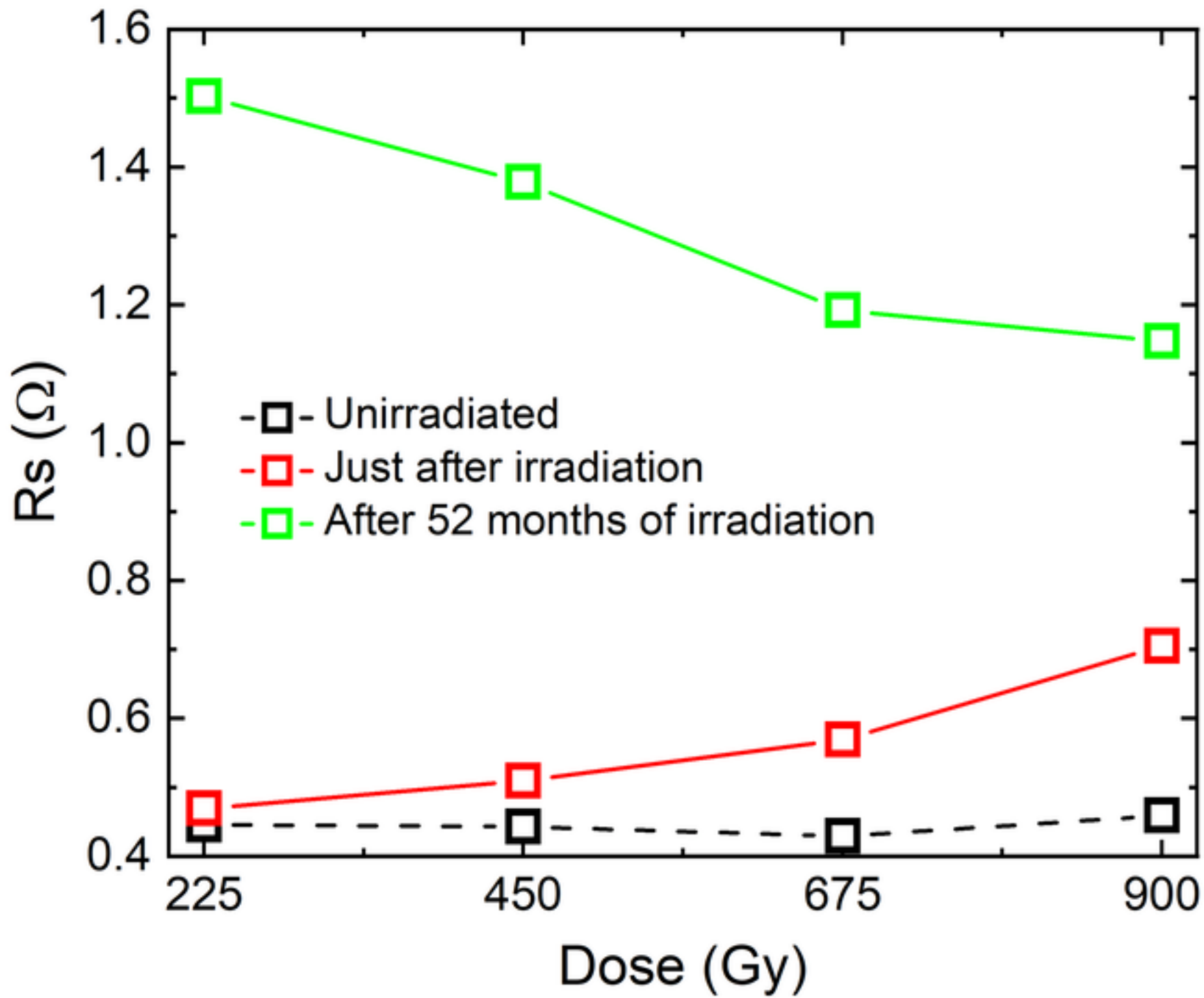
[Click here to access/download;Figure;Figure 4b.jpg](#)

Figure 5

[Click here to access/download;Figure;Figure 5.jpg](#)

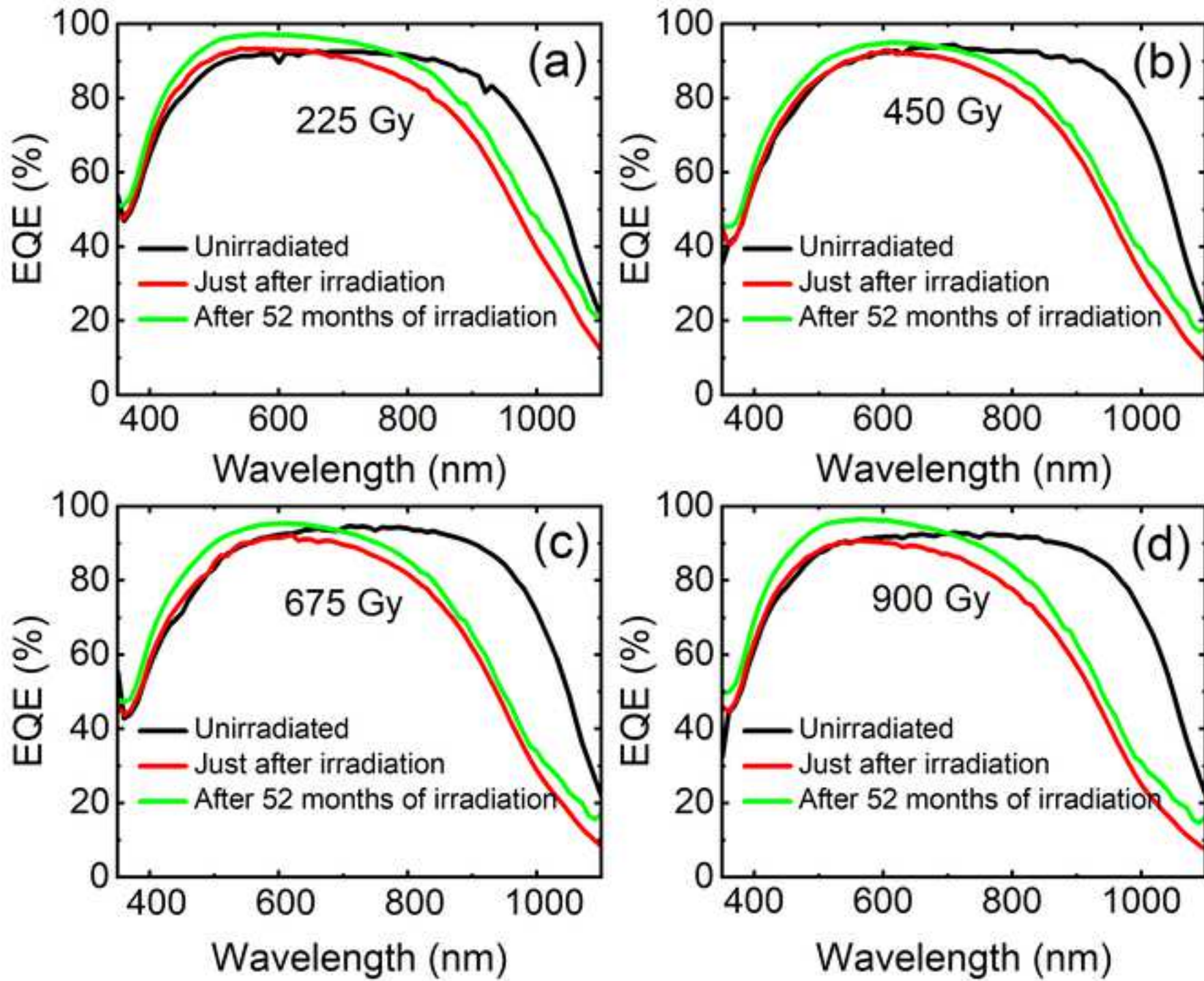


Figure 7

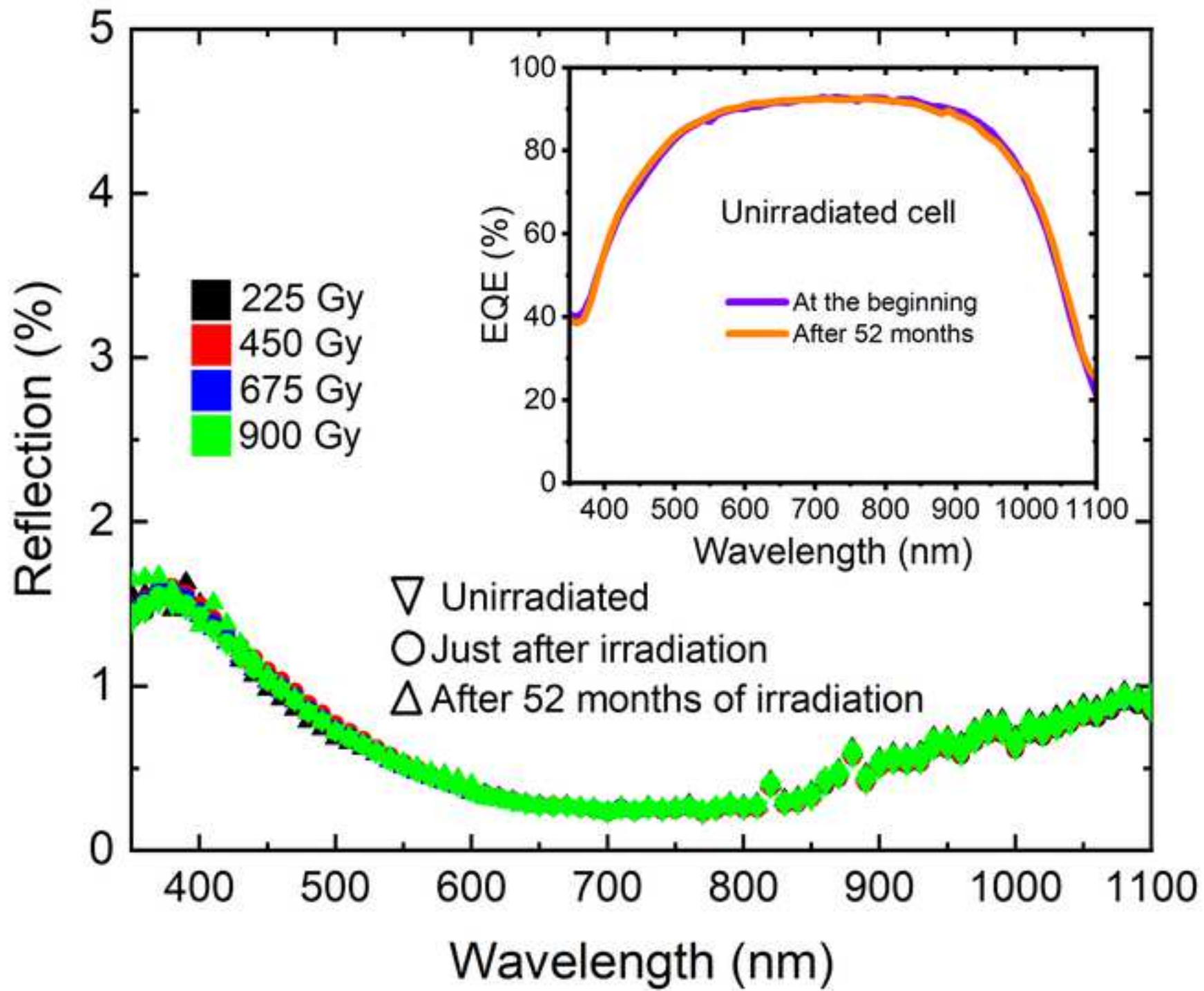
[Click here to access/download;Figure;Figure 7.jpg](#)

Figure 8

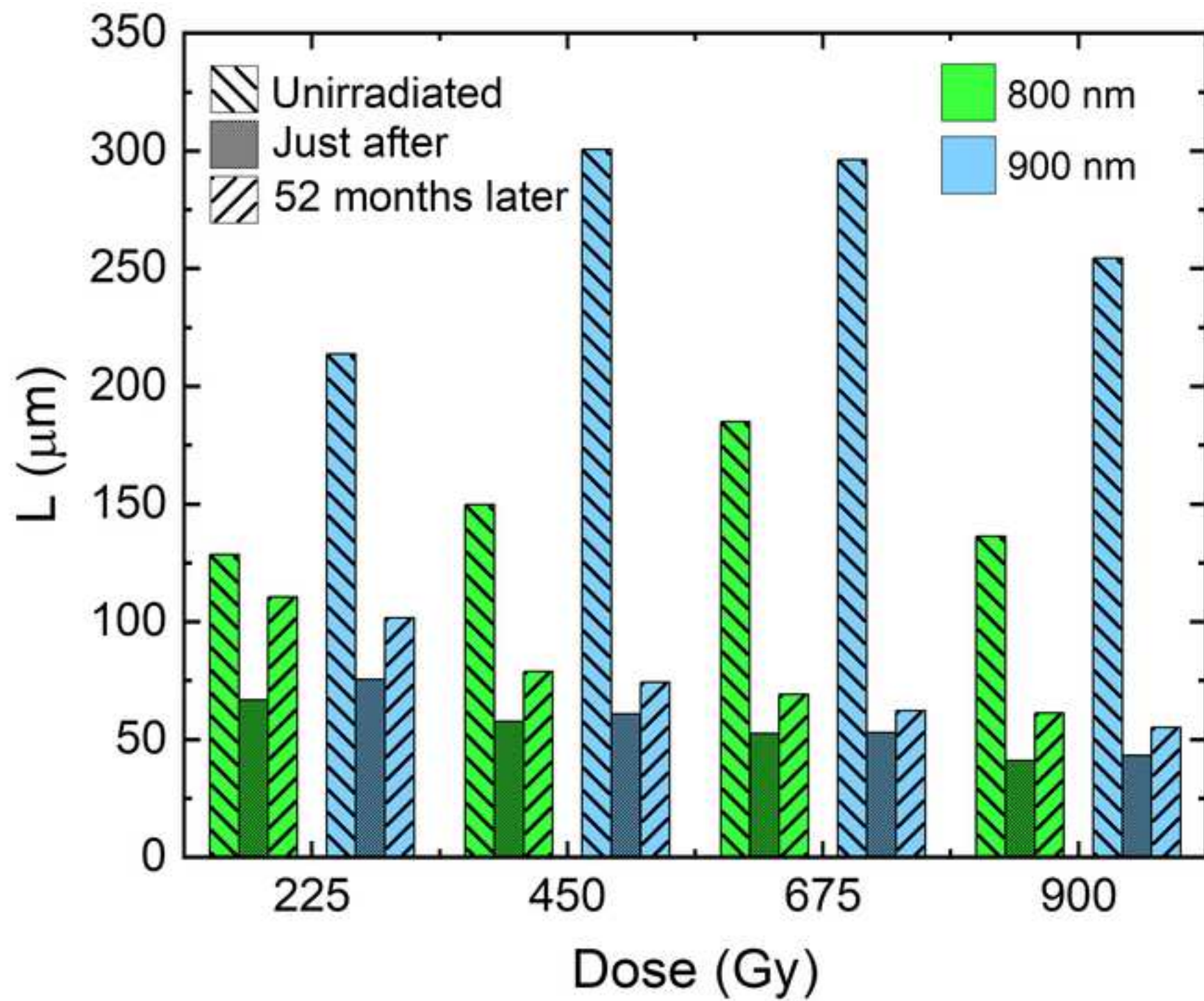
[Click here to access/download;Figure;Figure 8.jpg](#)

Figure 9

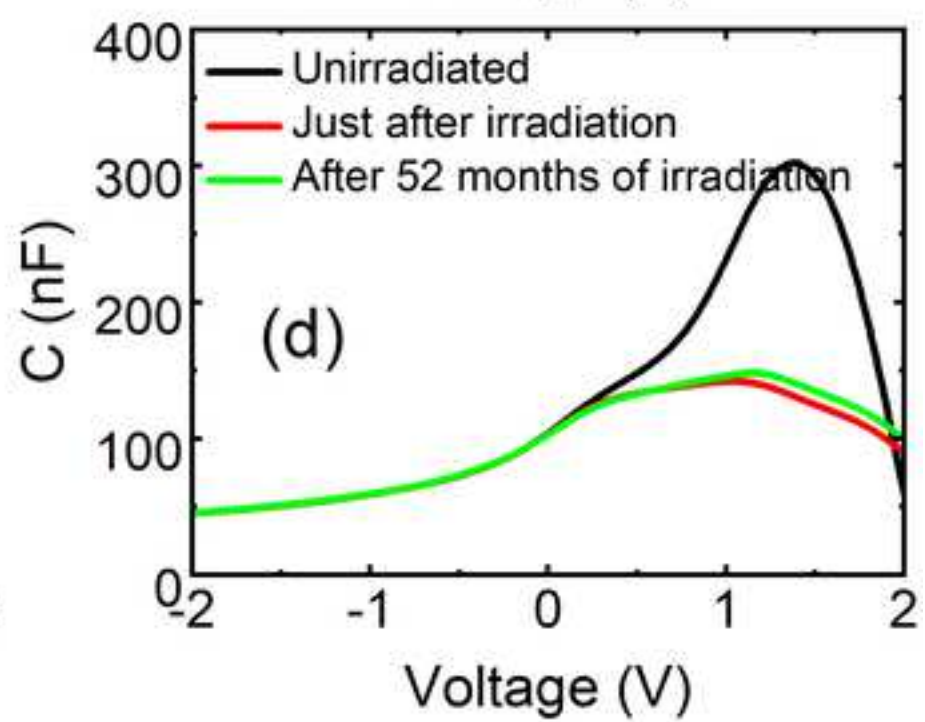
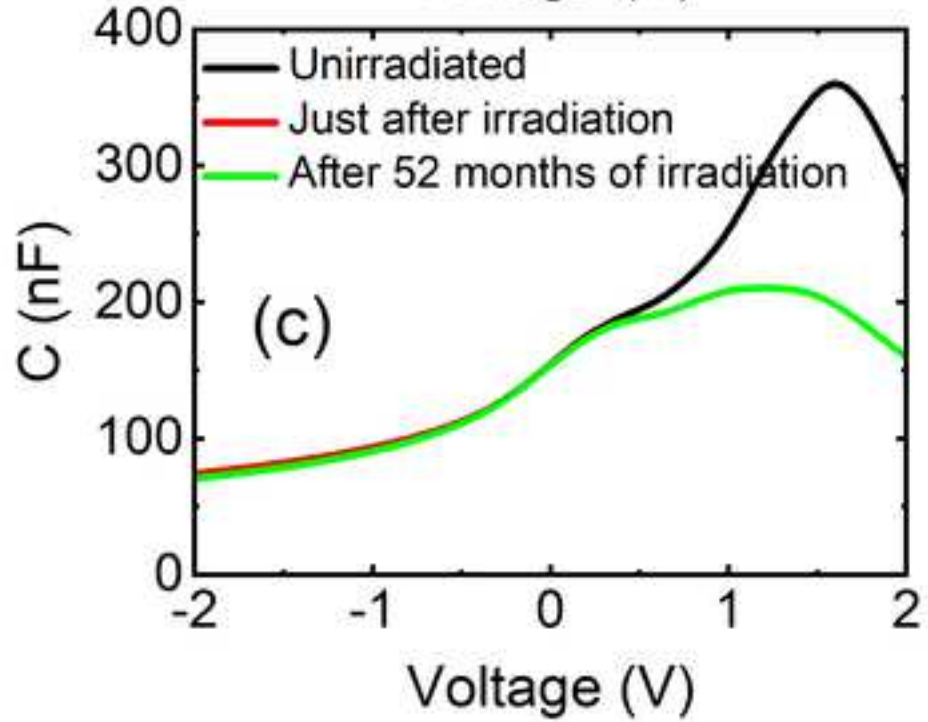
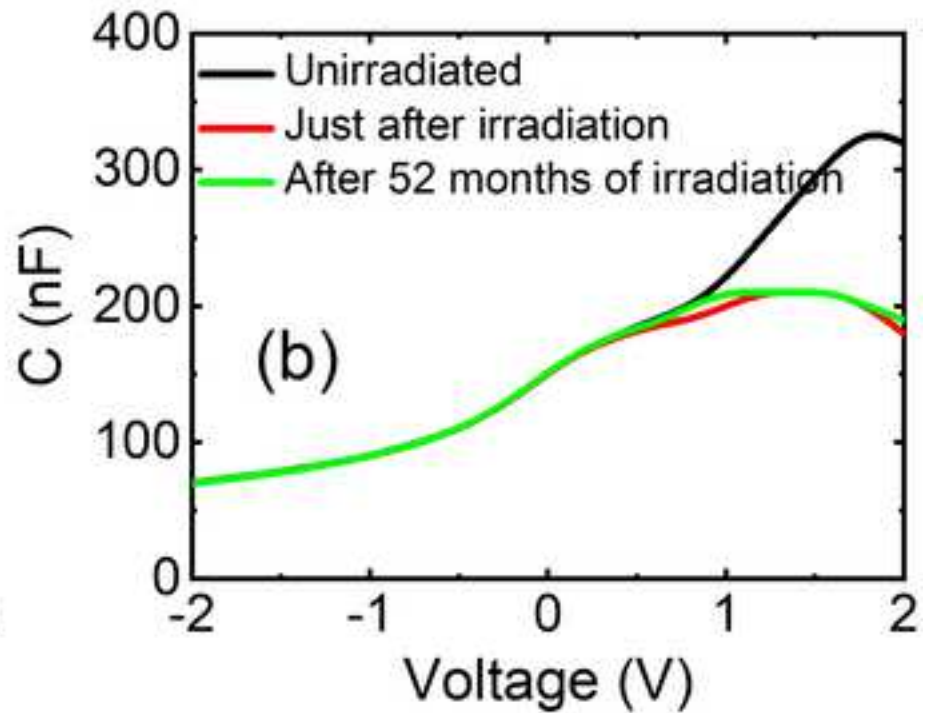
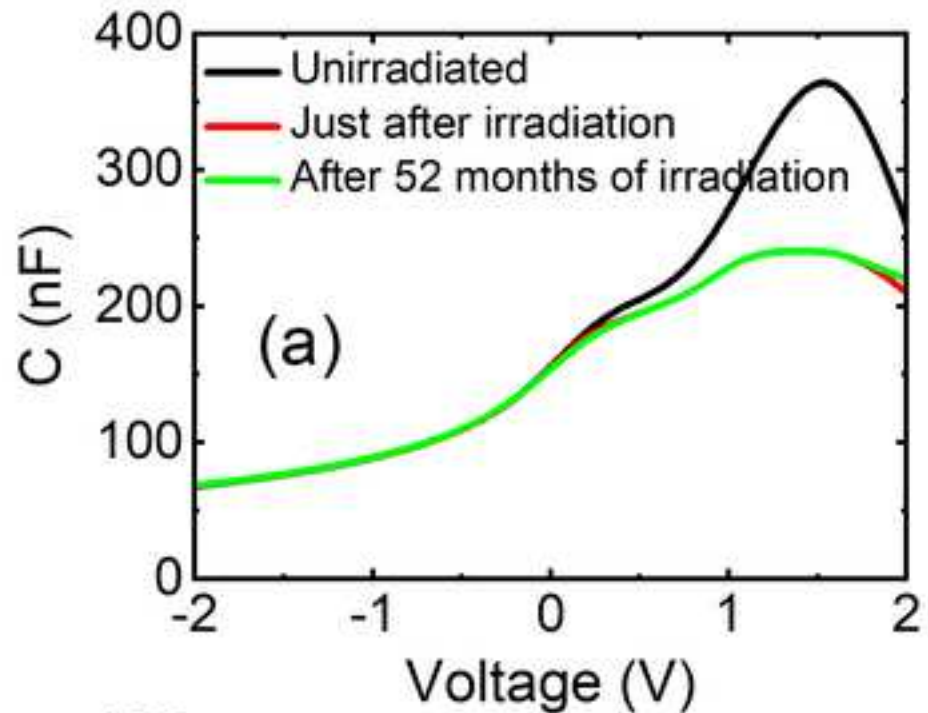
[Click here to access/download;Figure;Figure 9.jpg](#)

Figure 10

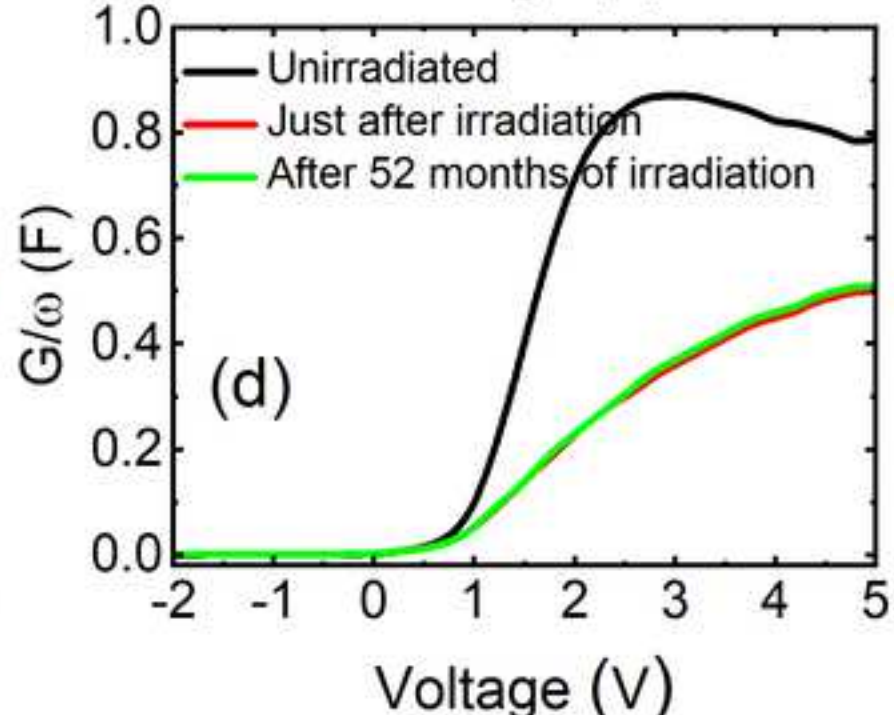
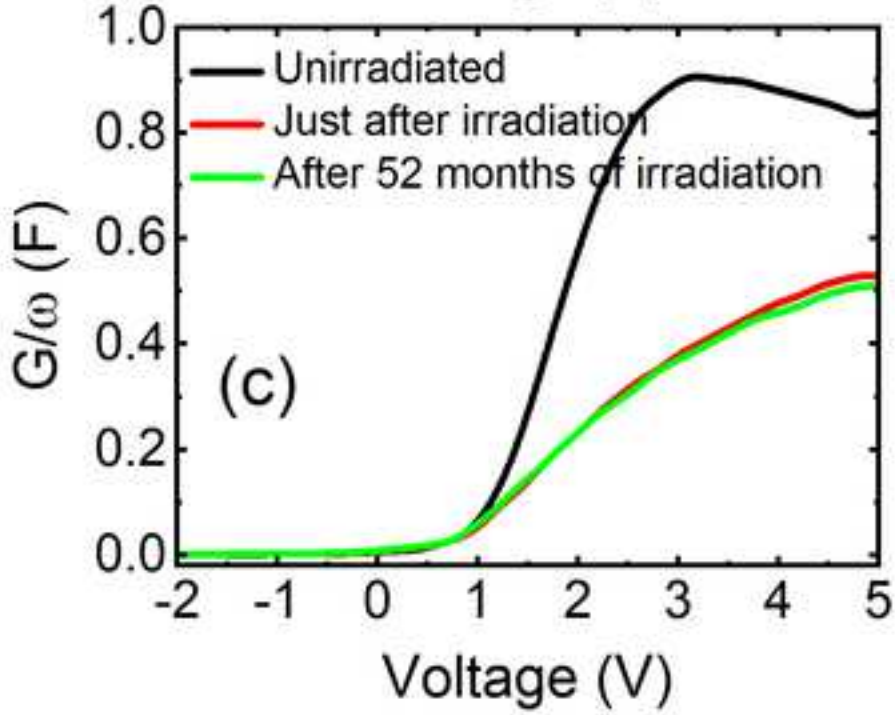
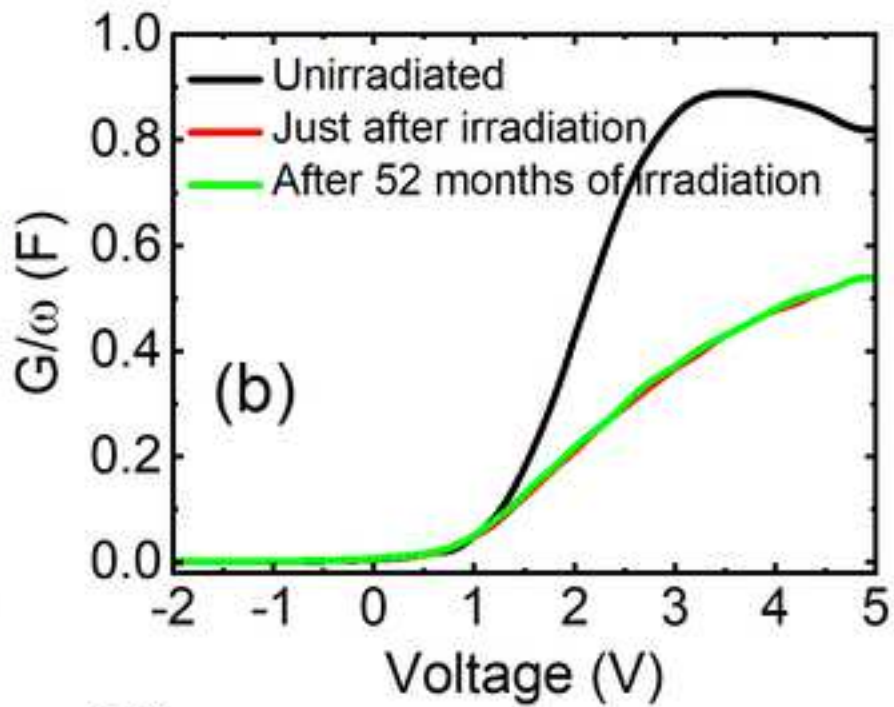
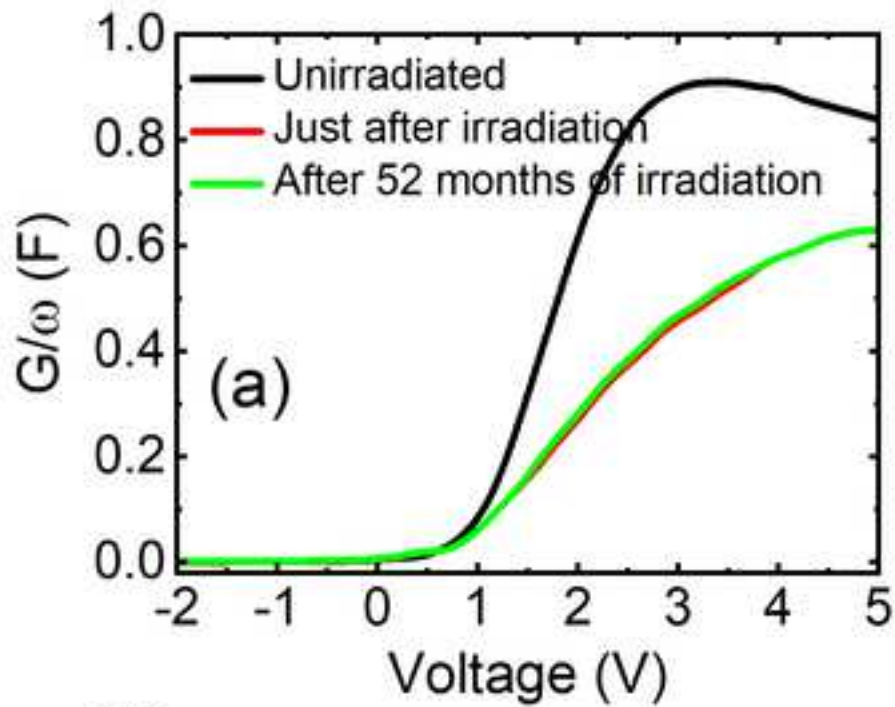
[Click here to access/download;Figure;Figure 10.jpg](#)

Table 1. Calculated diode parameters of the cells from measured dark I-V results.

Dose (Gy)	Unirradiated			Just after irradiation			After 52 months of irradiation		
	n ₁	n ₂	R _{sh} (Ω)	n ₁	n ₂	R _{sh} (Ω)	n ₁	n ₂	R _{sh} (Ω)
225	1.26	2.35	45561	1.34	2.51	13717	1.28	2.41	23797
450	1.28	2.37	58321	1.41	3.39	65316	1.41	2.36	85404
675	1.30	2.44	82353	2.00	3.92	4229	1.41	2.43	75404
900	1.47	1.65	3818	1.26	2.35	45561	1.43	2.31	22420

Table 2. Basic cell parameters obtained from illuminated I-V given in Fig.3

Dose (Gy)	Unirradiated				Just after irradiation				After 52 months of irradiation			
	Voc (mV)	Jsc (mA/ cm ²)	FF (%)	η (%)	Voc (mV)	Jsc (mA/ cm ²)	FF (%)	η (%)	Voc (mV)	Jsc (mA/ cm ²)	FF (%)	η (%)
225	578	36.7	77.1	16.3	553	31.9	78.7	13.9	558	34.4	62.9	12.1
450	586	35.6	74.9	15.6	542	29.3	76.5	12.1	546	31.2	63.7	10.8
675	580	35.8	76.5	15.9	538	28.8	76.7	11.9	540	30.4	69.5	11.4
900	585	34.6	77.8	15.7	534	26.9	78.4	11.3	537	27.9	73.4	10.9

Table 3. Calculated loss and recovery in J_{SC} values from illuminated I-V measurements (Fig. 2) for different radiation doses. J_{SC0} , J_{SC1} and J_{SC2} are the short circuit current densities of the cells before irradiation, just after irradiation and after a 52-month period of irradiation respectively.

Dose (Gy)	Loss in J_{SC} ($J_{SC0} - J_{SC1}$) (mA/cm ²)	Recovery in J_{SC} ($J_{SC2} - J_{SC1}$) (mA/cm ²)	Percentage in J_{SC} recovery (%)
225	4.70	2.47	52.6
450	6.37	1.92	30.1
675	6.97	1.62	23.2
900	7.60	1.23	16.2

Table 4. Calculated loss and recovery in J_{SC} values from EQE measurements (Fig. 5) for different radiation doses. J_{SC0} , J_{SC1} and J_{SC2} are the short circuit current densities of the cells for unirradiated, just irradiated and after 52 months of irradiation cases respectively.

Dose (Gy)	Loss in J_{SC} ($J_{SC0} - J_{SC1}$) (mA/cm ²)	Recovery in J_{SC} ($J_{SC2} - J_{SC1}$) (mA/cm ²)	Percentage in J_{SC} recovery (%)
225	2.75	2.24	81.5
450	4.62	1.73	37.4
675	5.36	1.89	35.3
900	5.87	2.60	44.3

Table 5. Percentage of loss and recovery in the diffusion length of electrons calculated at 800 and 900 nm.

Dose (Gy)	Percentage in Ln Loss (%)	Percentage in Ln Recovery (%)	Percentage in Ln Loss (%)	Percentage in Ln Recovery (%)
	800 nm		900 nm	
225	48	66	65	36
450	61	36	80	21
675	72	30	82	17
900	71	49	83	28